ANL-6865

Argonne National Laboratory

TERMINAL REPORT FOR THE MARK IV (PLUTONIUM) LOADING IN EBR-I

by

R. R. Smith, C. B. Doe,
R. O. Haroldsen, F. D. McGinnis,
and M. Novick

Printed in USA. Price $3.00. Available from the Clearinghouse for Federal Scientific and Technical Information, National Bureau of Standards, U. S. Department of Commerce, Springfield, Virginia

ANL-6865
Reactor Technology
(TID-4500, 45th Ed.)
AEC Research and
Development Report

ARGONNE NATIONAL LABORATORY
9700 South Cass Avenue
Argonne, Illinois 60440

TERMINAL REPORT FOR THE MARK IV (PLUTONIUM) LOADING IN EBR-I

by

R. R. Smith, C. B. Doe, R. O. Haroldsen,
F. D. McGinnis, and M. Novick

Idaho Division

April 1965

Operated by The University of Chicago
under
Contract W-31-109-eng-38
with the
U. S. Atomic Energy Commission

TABLE OF CONTENTS

TABLE OF CONTENTS

LIST OF FIGURES

LIST OF FIGURES

LIST OF TABLES

TERMINAL REPORT FOR THE MARK IV (PLUTONIUM) LOADING IN EBR-I

by

R. R. Smith, C. B. Doe, R. O. Haroldsen,
F. D. McGinnis, and M. Novick

I. INTRODUCTION

The recent successful operation of EBR-I with a plutonium loading terminated a long series of experiments, which began in August 1951 with initial criticality, and ended in December 1963 with decommissioning. During these years, the system operated with four separate and distinct loadings, three of which were fueled with fully-enriched U^{235} and the fourth and last, with metallic plutonium.

The first of these, Mark I, was fueled with cylindrical slugs of 93% enriched unalloyed uranium metal contained in stainless-steel, NaK-bonded jackets.[1-5] A decided loss in reactivity associated with a gradual fuel growth was correctly identified as the result of fast-neutron damage. Approximately 3.5×10^6 kWh of operation was accumulated before this loading was terminated.

To study the effects of alloying on radiation resistance, a second loading (Mark II) of fuel, consisting of uranium-2% zirconium alloy, was installed.[6] As anticipated, the inclusion of this small fraction of zirconium resulted in a significant increase in the integrity of the fuel. A final phase of the experimental program was devoted to the analysis of the dynamic reactor performance under various conditions of power and flow.[7] Upon completion of these experiments, operation of the reactor was to be terminated and the reactor was to be placed in standby status. One of a number of transient experiments conducted with the main coolant flow stopped, demonstrated conclusively the existence of an overall, prompt, positive power coefficient of reactivity and led inadvertently to a partial melting of the reactor core.[8,9] As a consequence of this incident, considerable concern was expressed for the safe operation of future fast-spectrum breeder reactors.

To prove there was nothing intrinsically unsafe in the operation of such a system, the damaged core was replaced with a loading (Mark III) specifically designed and sufficiently flexible to study, in detail, feedbacks arising from fuel, coolant, structure, and rod deformation.[10] As the result of a comprehensive experimental program, concerned mainly with

transfer-function and power-coefficient measurements, it was concluded that those features responsible for the instability noted in the earlier loadings could be eliminated by rather elementary changes in mechanical design.(11-13)

The operation of the Mark IV core, fueled entirely with plutonium, introduced a variety of problems which required careful scrutiny before loading and eventual operation.(14) Although many problems were of a more or less conventional nature, others were complicated by physical, chemical, and neutronic properties peculiar to plutonium. The low melting point of the fuel, the tendency to deform under stress, its toxicity, and the small value for β_{eff} constituted sources of hazard not usually encountered in U^{235}-fueled systems.

In retrospect, the most immediate benefit resulting from the refueling and operation of EBR-I with plutonium is the reassurance that there is nothing inherently unsafe or dangerous in the operation of a plutonium-fueled system. Of a less tangible nature are the benefits that come from practical experience, as, for example, the actual handling of the fuel and the routine day-to-day startups and shutdowns of the system. Such assurance assumes added significance when it is realized that, at one time, the operation of EBR-I was characterized by instability problems. The eventual elimination of the source of instability, and the successful operation with plutonium fuel, conceivably could influence the siting of future fast reactors.

More tangible benefits of the Mark IV experiments may be found in the results of two series of measurements: an analysis of the dynamic characteristics of the system,(15) and an evaluation of the breeding ratio.(16) A discussion of these results, along with summaries of observations relevant to routine reactor operations, constitutes the subject of this report.

II. DESIGN

A. The Necessity of a Liquid-metal Coolant

Most power-producing fast systems currently in operation or envisioned for future use are characterized by a common distinguishing feature, the use of a liquid-metal coolant. Usually, molten sodium or an alloy of sodium and potassium, NaK, is used for this purpose. Both have excellent heat-transfer properties which permit the efficient removal of heat from small, high-power, density systems. What is more important, however, is the necessity for perpetuating the chain reaction with essentially unmoderated fission neutrons. Unless the neutron spectrum is "hard," an intolerably large fraction of neutrons undergoes parasitic capture in the fuel, coolant, and structure. The use of NaK or Na assures a high-energy spectrum and, consequently, a satisfactorily high breeding ratio.

B. Description of the System

Although details pertaining to the reactor and auxiliary components have been previously given,[14] it is nevertheless instructive to review those features that promote a general understanding of the EBR-I system.

The reactor is unmoderated and heterogeneous and was designed for full-power operation at a thermal output of approximately 1 MW. To permit the efficient removal of heat under high-power density conditions (180 kW/liter), and to minimize neutron moderation, a potassium-sodium eutectic (NaK) is used as a coolant.

The coolant flows under gravity from an elevated supply tank downward through a low-density inner blanket, upward through the core, through a primary-secondary heat exchanger, and into a receiving tank in the basement. A pump, operating at a capacity slightly greater than the main coolant flow, returns the coolant to the gravity supply tank. An overflow system, connected from the supply tank to the receiver, guarantees a constant level of delivery.

Heat from the secondary coolant (also NaK) may be removed in either of two ways: through the generation of steam, which is used to drive a conventional turbine-generator, or through a fan-cooled load dissipator. Because the primary coolant is intensely radioactive during operation and immediately following shutdown, all primary components are enclosed in concrete-shielded cells. The secondary coolant, on the other hand, is nonradioactive and, accordingly, requires no shielding.

Of the total thermal power generated in the system, approximately 16% is produced in a massive movable reflector which surrounds the primary reactor tank. The reflector originally consisted of an assembly

of stainless-steel-clad, keystone-shaped, uranium bricks. The entire assembly, weighing approximately 5 tons, is mounted on a pedestal which may be raised or lowered relative to the core. A forced circulation of air through finned-cooling holes in the bricks removes heat generated through fission and gamma absorption. Twelve stainless-steel-clad uranium rods, which penetrate holes in the vertical columns of bricks, serve as safety or control rods. The reflector serves three purposes: as a dense breeding medium for the conversion of U^{238} to Pu^{239}, as a coarse control of reactivity, and as a means of rapid reduction in reactivity in the event of a scram signal.

The inner tank assembly consists of several hexagonally-shaped, stainless-steel subassemblies, filled either with fuel or blanket rods. Fuel rods in Mark IV consist of a fuel region, consisting of slugs of Pu-1.25 w/o Al alloy, and upper and lower blanket regions, containing slugs of depleted uranium. Blanket rods located between the fuel region and the structure rings contain fertile material only.

1. Coolant Systems

The primary and secondary systems contain a NaK eutectic which, with a melting point of -12.5°C, is liquid at room temperature. The primary coolant flows under gravity from an elevated supply tank, through the inner blanket and core, through a primary-secondary heat exchanger, into a receiving tank in the basement. One of two pumps (one d.c. electromagnetic and one mechanical centrifugal) returns the coolant to the gravity supply tank at a rate somewhat greater than reactor flow. An overflow system connecting the supply reservoir to the receiving tank guarantees a constant-pressure head and continuous mixing of the contents of both tanks. Variations in inlet flow are eliminated, and the large capacity of the tank (2700 gal) assures a holdup time long enough to smooth out minor variations in reactor inlet temperature. Various components and their relationship with one another are illustrated in Fig. 1. From the viewpoint of safety, the gravity tank provides approximately 9 min of full coolant flow in the event of pump failure. If necessary, flow from the gravity tank may be throttled to provide up to 8 hr of flow at a rate sufficient to remove decay heat. A small fraction of the pumped flow is by-passed through a filter clean-up system.

The activation of sodium in the coolant during its passage through the core results in the formation of Na^{24}, a 14.7-hr, hard beta-gamma emitter. Accordingly, all primary components are located in concrete-shielded cells. Such areas are completely inaccessible during operation but may be entered on a limited basis after a sufficient decay period.

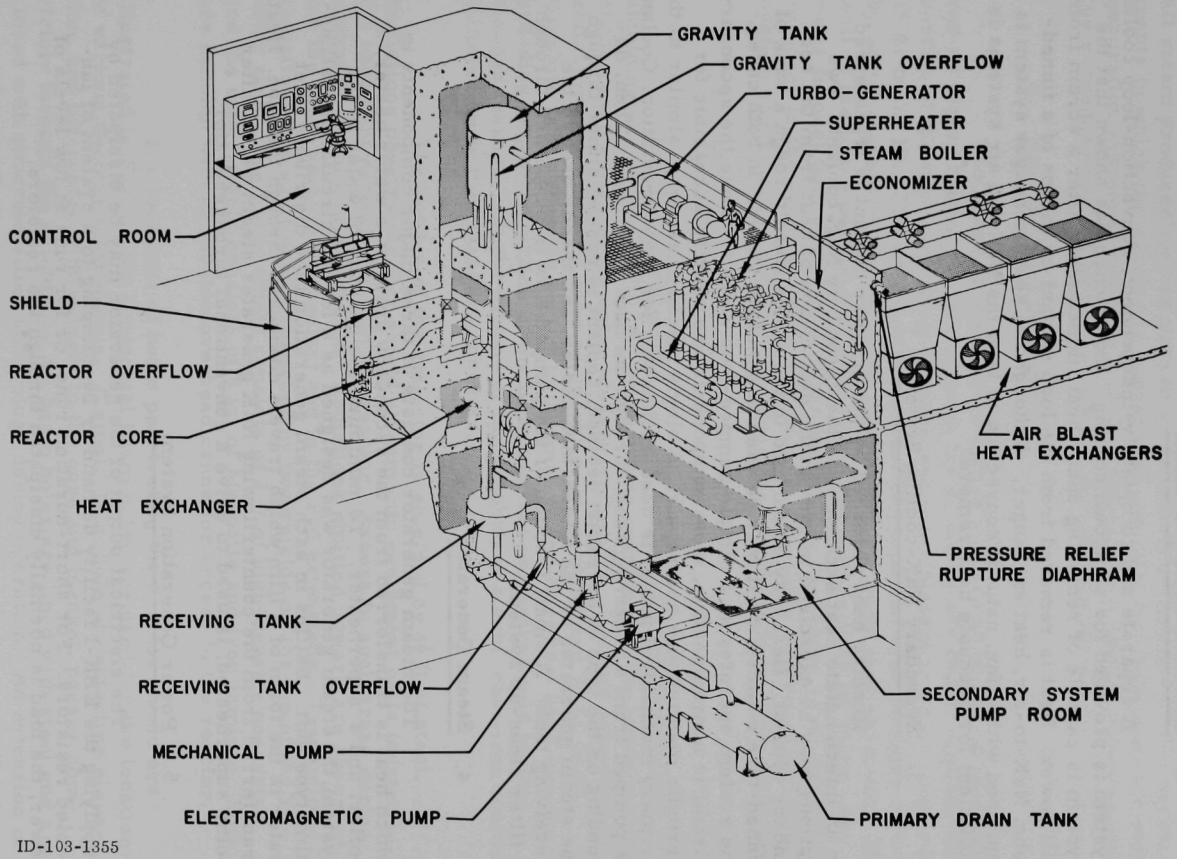

Fig. 1. Reactor System, EBR-I

2. Shutdown Cooling Systems

A separate and completely-independent, convection-loop cooling system is provided for shutdown cooling. Experience has shown that the system is capable of removing decay heat immediately after a scram from full power. Heat is removed from the loop coolant by means of a finned-tube, NaK-to-air, heat exchanger. Although the heat exchanger system is equipped with a fan, natural convection in both the NaK and air systems is sufficient for adequate heat removal.

3. Secondary NaK-cooling System

Reactor heat absorbed by the primary coolant is transferred in an intermediate heat exchanger to the secondary NaK coolant. Two options may be exercised in turn in the dissipation of heat from the secondary coolant. Heat may be dumped to the atmosphere through a bank of finned-tube coolers, or it may be used to generate steam. In both cases, the system operates as a simple pumped-loop circuit. Since the secondary circuit is nonradioactive, most components are readily accessible for periodic maintenance and repair. A single mechanical pump, similar to the primary mechanical pump, is used exclusively for loop circulation. Coolant is pumped from a receiving tank, through the heat exchanger. Then, depending on the type of operation desired, coolant is passed either through the steam generator or the finned-tube cooler, and thence back to the receiving tank. A small fraction of the pumped flow is by-passed through a filter clean-up system.

4. Steam Generator

The steam generator consists of three major components in which heat is transferred from the secondary system: a water heater, a boiler, and a superheater. To minimize the quantity of water in the system, the steam generator was designed as a forced-circulation, falling-film-type unit. Baffles in each steam generation tube distribute inlet water in the form of a film which travels downward through the tube. Heat transferred from the counterflowing NaK generates steam which, after being superheated, is used to drive a conventional turbogenerator.

5. Power Generation System

The electrical output of the generator may be dissipated by supplying the EBR-I facility demand or by dumping to a system of fan-cooled resistors. For short-duration runs, or for runs at low levels of power, the load is normally dissipated through the resistors.

When energy is dissipated by assuming the facility load, the reactor power is held constant. Any excess steam is exhausted to the

turbine condenser through back-pressure-regulating valves. If necessary, all steam produced may be passed directly to the condenser. For experiments in which the reactor is operated at low inlet temperatures, the steam generation system is bypassed. In this special case, heat is removed from the secondary coolant by the air-cooled, finned-tube system.

6. Reactor Tank Assembly

The shape of the reactor tank is illustrated in Fig. 2. The tank and all piping leading from it through the shielding are double-walled. The portion of the tank containing the core and inner blanket is 28 in. long and 15.87 in. in ID. The weight of the vessel is supported by a shoulder formed by an increase in diameter at the junction of the lower tank assembly. The wall of the lower portion of the inner reactor tank is 5/16 in. thick. An outer Inconel tank with a wall thickness of 1/16 in. serves as an emergency receiver in the event of inner-tank failure. The tanks are separated by a system of ribs running vertically along the inside surface of the outer tank.

7. Shielding

Horizontal and vertical cross sections through the reactor shielding are shown in Fig. 2. Immediately surrounding the lower portion of the reactor tank is the outer blanket (reflector). Located outside the reflector is an annular layer of graphite, 18 in. thick and 35 in. high. Graphite is used in this region to thermalize and to reflect back into the breeding region a fraction of the neutrons that normally would be lost through leakage. On the outside of the graphite is a 4-in. cast-iron course, followed by $8\frac{3}{4}$ ft of standard concrete.

The bottom of the reflector is shielded by $4\frac{1}{2}$ ft of steel. Radiations penetrating this shield stream into equipment cells located in the basement directly beneath the reactor. Access to such areas during operation is, of course, denied. Radiations emitted upward are absorbed, for the most part, in the coolant and in the rod extensions. Transmitted radiations are additionally absorbed by two shields on the top of the reactor tank. The lower shield consists of 2 ft of high-density concrete, and the upper shield consists of 8 in. of Masonite and iron laminae. Both are handled with the 20-ton overhead crane for access to the reactor.

The locations of holes penetrating the reactor shield are illustrated in Fig. 2. Six horizontal beam holes are used for the location of various nuclear instruments. A single 3-in. hole at centerline elevation, and off-center with respect to the core and blanket, passes completely through the shielding. All beam holes are lined with steel and are closed with concrete-filled steel plugs during operation. An extension of the graphite reflector into the concrete shielded region serves effectively as a thermal column.

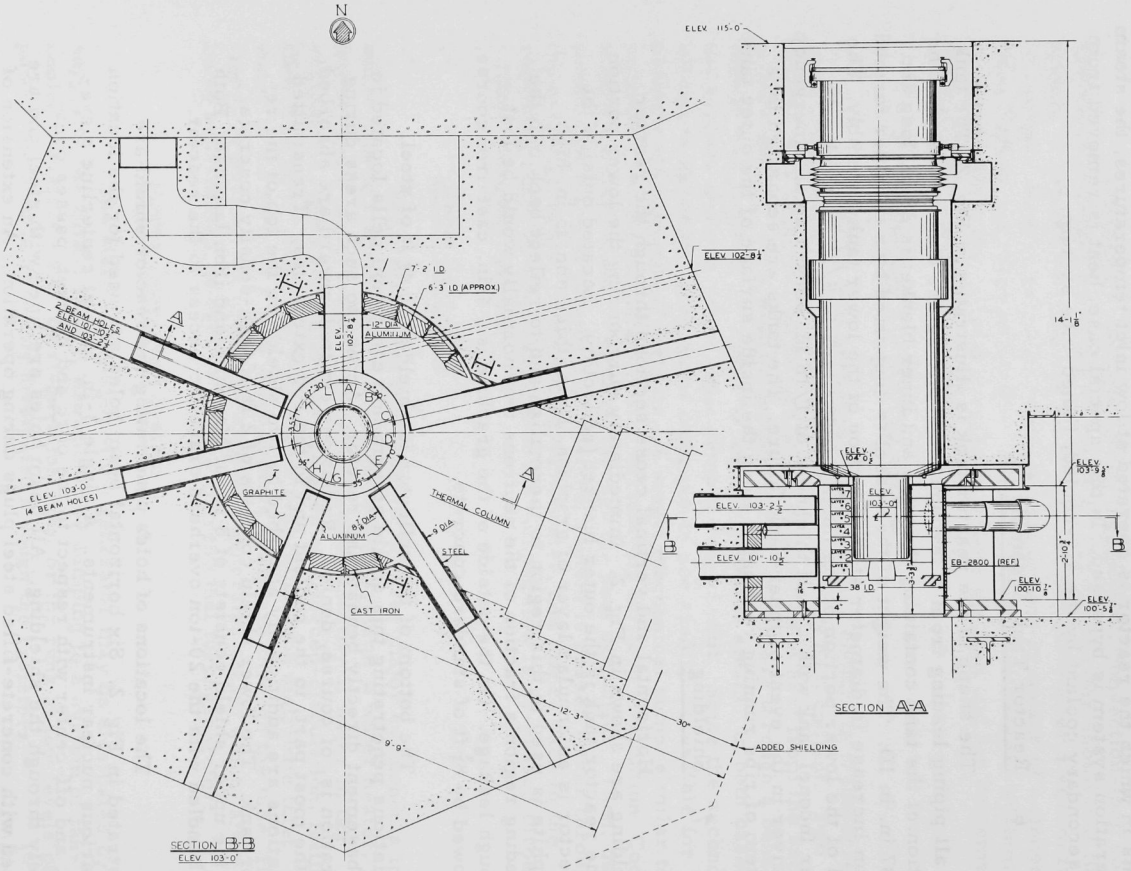

103-405

Fig. 2. Horizontal and Vertical Cross Section through Shield

Five vertical holes penetrate the graphite reflector from the reactor top. These may be used for the irradiation of specimens in a reasonably-well-thermalized neutron flux. Special thimbles designed for installation in the core or inner blanket regions are provided for the irradiation of specimens in a fast-neutron atmosphere.

8. Ventilation and Cooling Systems

The reactor air supply and outer-blanket-cooling and shield-cooling exhaust systems are interconnected. A blower provides the supply air which is taken from the outside of the building and forced through an electrostatic filter. Cooling air for the shield is pulled from the supply plenum by a centrifugal blower located on the outlet side of the shield-cooling system. Before its release through the exhaust stack, the cooling air is passed through a bank of high-efficiency filters.

The reflector cooling system also receives air from the same plenum. A positive-displacement blower draws air downward through cooling holes, through the reflector-support shielding, through teloscopic tubes in the elevator structure, and into a plenum chamber. From here it is drawn through high-efficiency filters and released through the stack.

9. Cover Gas System

All NaK storage tanks, both mechanical circulating pumps, and the top of the reactor operate under a controlled atmosphere of purified argon at a pressure of approximately 5 $lb/in.^2$. A similar system operating at a slightly higher pressure is associated with the secondary NaK system.

Feed gas, consisting of welding-grade argon, is passed through pressure-reducing valves to a purifier, which consists of a stainless-steel mesh-packed column of heated NaK. Impurities of oxygen and water are removed through chemical action with the NaK.

10. Reactor Instrumentation

A block diagram outlining the various channels of nuclear information is shown in Fig. 3. Nonnuclear information pertinent to the operation of the various systems is gathered by conventional instrumentation and is displayed in the control room visually or is registered with chart recorders. Details regarding the many items of equipment are summarized in Ref. 14.

11. Control- and Safety-rod Drive Systems

There are 12 stainless-steel-jacketed, natural uranium rods, each 2 in. in diameter. All 12 rods move vertically in holes penetrating the

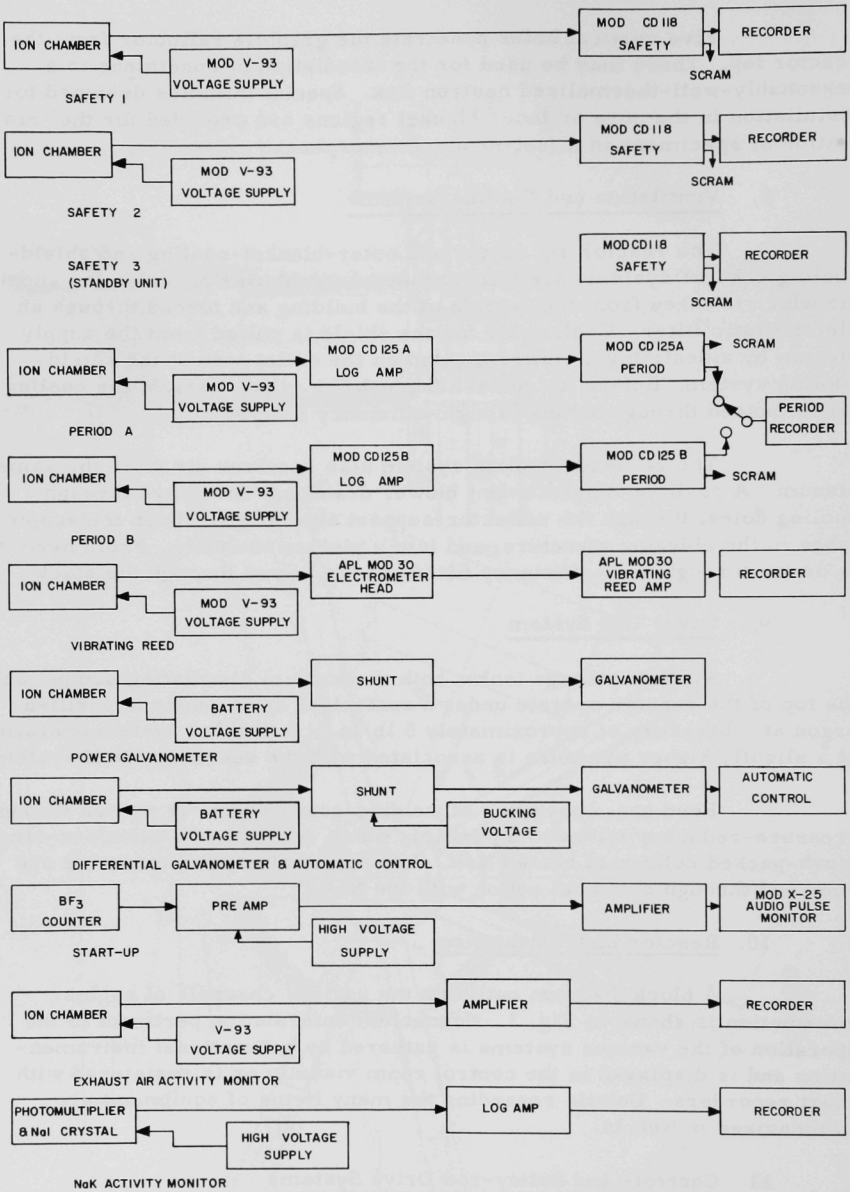

Fig. 3. Reactor Nuclear Instrumentation

reflector. Eight of the 12 serve as safety rods and are driven upward into the reflector before startup by a rack and pinions driven through a magnetic clutch. An interlock device requires that all eight safety rods be fully inserted before the reflector can be raised to a predetermined position. The rods are driven upward against springs which act to force the rods downward upon an interrupt signal to the magnetic clutches. The four control rods are connected to lead screws which are raised and lowered through V-belt-driven gear boxes. These cannot be scrammed and, accordingly, do not participate in a fast shutdown. Each of the 12 rods is worth approximately 3×10^{-4} $\Delta k/k$.

The reflector is mounted on a hydraulically-driven platform, which may be raised or lowered relative to the core. Movement of the reflector in its total travel between the fully down and fully up positions is worth approximately 5% $\Delta k/k$. The elevator mechanism and the shielding section upon which the reflector rests are illustrated photographically in Fig. 4.

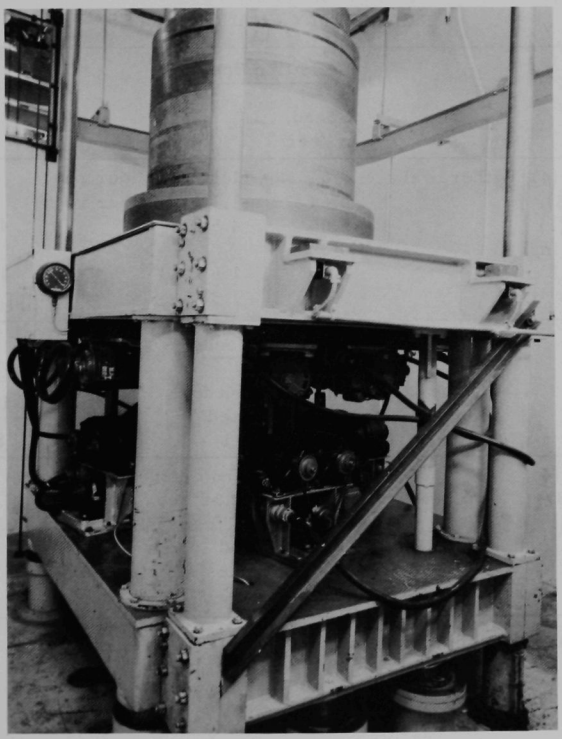

ID-201-237

Fig. 4. Elevator Assembly Showing Lower Shield

An additional control of reactivity is provided by a tapered uranium plug which makes up the bottom of the reflector and which may be driven pneumatically into and out of it. The reactivity worth of the safety plug in its travel between maximum and minimum worth positions (a distance of 6 in.) is approximately 0.054% $\Delta k/k$.

The total travel of the reflector is 80 in. The elevation rate for the first 50 in. is 0.32 in./sec. Between 30 and 5.15 in. from the top of travel, the elevation rate is slowed to 0.095 in./sec. At 5.15 in., the elevator comes in contact with motorized stops, and the elevation rate between this point and the top of travel is additionally slowed to 0.005 in./sec. An interlock system requires that the motorized stops be driven downward to the 5.15-in. position before the elevator may move past this point. Reactivity insertion and withdrawal rates, based on experimental measurements with the natural uranium reflector in place, are summarized in Table I.

Table I

REACTIVITY CHANGE RATES*

Addition Speed

	Speed, in./sec	$\Delta k/k/sec$	Ih/sec
Control Rods (4), withdrawal	0.64	1.1×10^{-5} per rod	1.00 per rod
Safety Rods (8)	0.64	1.1×10^{-5} per rod	1.00 per rod
Safety Block (1)	5.00	4.5×10^{-4}	42.8
Cup (80 to 30 in.)	0.32	--	--
Cup (30 to 5.15 in.)	0.095	1.6×10^{-4}	15.2
Cup (5.15 to 0 in.)	0.005	1.38	1.31

Scram Speeds

	Time to Initiate Motion, sec	Total Time for Indicated Travel	Reactivity Change		
			% $\Delta k/k$	$	Inhours
Control Rods (4)		No scram provision			
Safety Rods (8)	0.085	0-16 in., 0.38 sec	0.18	0.61	177
Safety Block (1)	0.15	0-6 in., 0.35 sec	0.054	0.18	51.3
Cup	0.10	0-5.15 in., 0.31 sec	1.38	4.66	1310
		0-12 in., 0.56 sec	4.21	14.2	4000
		Total travel	5.82	19.7	5528

*Cup calibrations based on uranium cup.

$\beta = 0.00296$.

12. Interlock System

Interlock switches and devices have been incorporated into the various auxiliary systems to guarantee that operational conditions cannot vary beyond predetermined limits of safety.

The interlock philosophy concerns three categories of action to be taken upon receipt of a malfunction signal. The most serious conditions are indicated on an annunciator panel by a red light. Action in this case is automatic and is manifested by an immediate fast shutdown (scram). Upon the receipt of such a signal, hydraulic pressure in a piston, holding the pedestal and reflector, is relieved by opening solenoid valves to a supply reservoir. The entire reflector assembly, worth at least 4% $\Delta k/k$, falls away from the lower tank assembly and shuts the reactor down.

A less severe malfunction is indicated by an amber light. In this case, action must be taken to correct the malfunction within 2 min or the reactor will automatically shut down. The third and final category is essentially for minor irregularities which require attention but which are not considered serious enough to warrant an immediate shutdown. Such irregularities are announced by a blue light on the annunciator panel. A malfunction in any category is announced by a Klaxon horn, which is silenced by pressing an acknowledge switch.

C. Inner Tank Assembly

The inner tank assembly of the Mark IV reactor is the same as that used in the Mark III reactor and consists of the supporting structure, core clamps, coolant plenums, flow control valves, etc., and 19 hexagonal cross-section-shaped boxes in the center, arranged in a hexagonal array. Seven new central boxes constitute the "reactor core," and the surrounding 12 boxes constitute the "inner blanket." Each core box is designed to contain 60 fuel rods and one central tightening rod. Of the 420 spaces for fuel therefore available, the ones over and above those required for fuel rods are filled with rods containing depleted uranium.

The outer boxes each contain 36 blanket rods and a central tightening rod. These rods enclose natural uranium, which constitutes the inner blanket, and are the same as the ones that were used in the Mark III loading.

1. Fuel Core Blanket Rods

Details of a typical Mark IV fuel rod are shown in Fig. 5. Fuel and core blanket material is in the form of metallic slugs arranged end-to-end in Zircaloy-2 jackets. The jackets have an OD of 0.299 in. and a wall thickness of 0.021 in. Three equispaced ribs, each 0.049 in. in diameter,

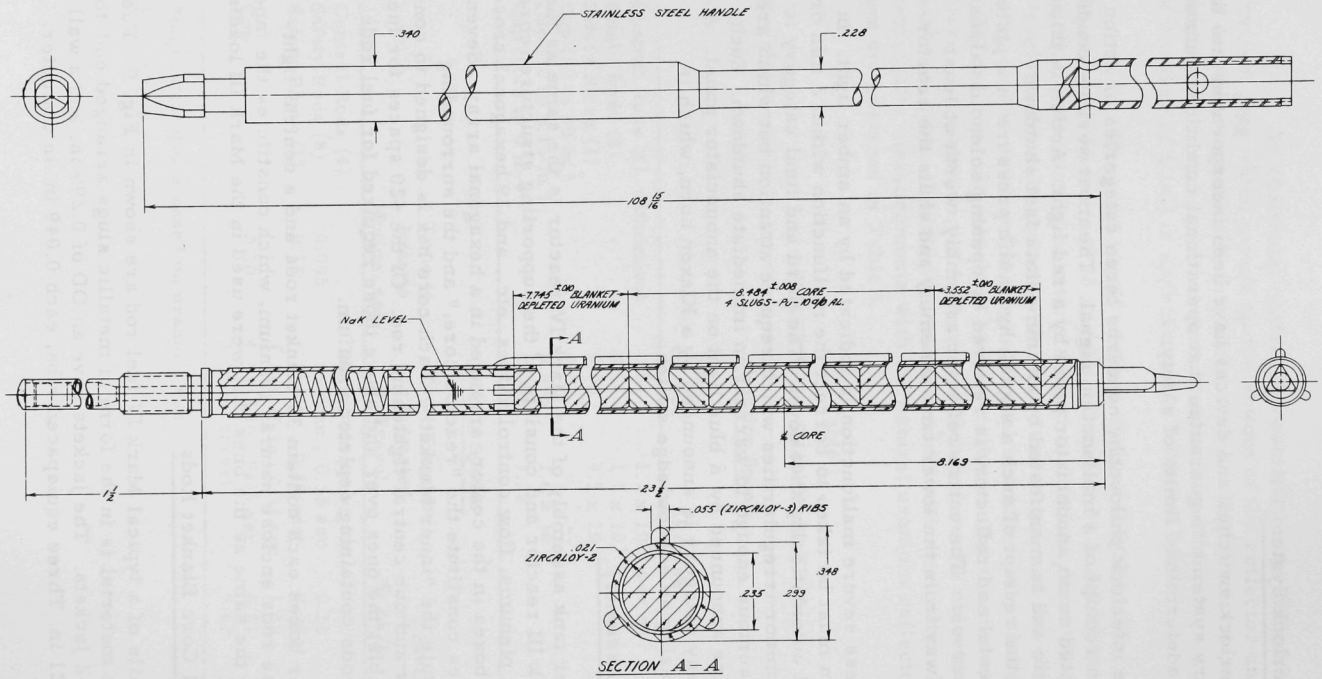

103-407

Fig. 5. Mark IV Fuel Rod

run longitudinally along the active portion of the rod. The ribs serve three functions: to provide uniform spacing, to assure maximum radial coupling, and to prevent or limit inward rod-bowing effects.

2. Fuel Material

The fuel material consists of an alloy which has the following weight compositions: Pu, 98.59%; Al, 1.25%; and impurities (Fe, Cr, Ni, and Cu), 0.16%.[14] On an atomic basis, this composition is equivalent to 90.0 a/o plutonium, and 10.0 a/o aluminum. The fuel was fabricated from two batches of feed material. One batch (the larger) had the following isotopic composition: Pu^{239}, 95.1 ± 0.01%; Pu^{240}, 4.5 ± 0.1%; Pu^{241}, 0.44 ± 0.01%; and Pu^{242}, a trace. The second batch had the following composition: Pu^{239}, 93.2 ± 0.1%; Pu^{240}, 6.2 ± 0.1%; Pu^{241}, 0.55 ± 0.01%; and Pu^{242}, a trace. An average composition established through inventory figures resulted in the following weight percent values: Pu^{239}, 94.4%; Pu^{240}, 5.1%; Pu^{241}, 0.5%; and Pu^{242}, a trace.

The average density of the alloy was measured to be 15.03 ± 0.05 g/cm^3, and its melting point is approximately 790°C. The coefficient of linear expansion over the temperature range 20-425°C amounts to 12.5 x 10^{-6} $\Delta L/L°C$. The thermal conductivity of an alloy consisting of Pu-1 w/o Al (close to that of the Mark IV composition) varies from 0.022 cal/(cm)(sec)(°C) at 100°C to 0.038 cal/(cm)(sec)(°C) at 400°C.

One of the most important design criteria to be satisfied consists of a conservative limitation of 450°C imposed on the maximum fuel temperature. This requirement is a consequence of two separate effects. One is an increased tendency for the fuel material to flow (slump) under self-compression for temperatures above 500°C. The other is concerned with a phase transition of δ to $\delta + \epsilon$ at approximately 700°C. (See phase diagram, Fig. 6.)

The fuel portion of the rods consists of four plutonium-aluminum alloy slugs each 2.121 in. long, giving a total core height of 8.484 in. Depleted uranium slugs, 7.745 and 3.552 in. long, located above and below the fuel portion, define the upper and lower breeding blankets, respectively. All fuel slugs are 0.232 in. in diameter, and all blanket slugs are 0.235 in. in diameter. Die-formed ribs on the surface of the fuel slugs position the slugs concentrically in their jackets. A cross-sectional view through the fuel section of a typical Mark IV fuel rod is shown in Fig. 7. The ribs were not rolled into the surface of blanket slugs; a series of four "stakes" at upper and lower ends served as a positioning mechanism.

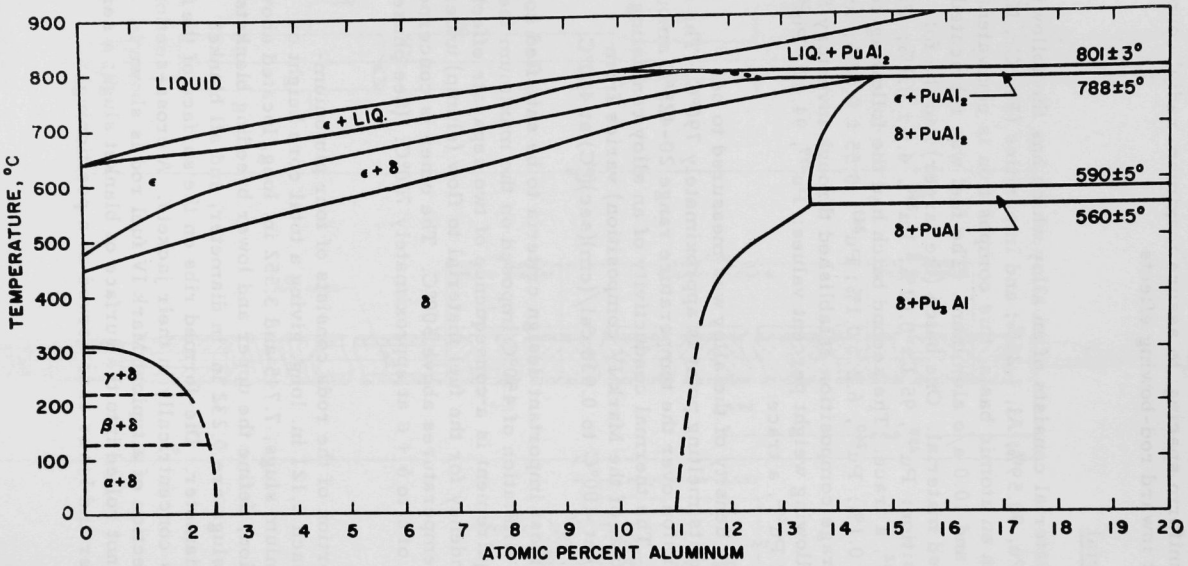

NOTES

1. $\frac{1}{4}$ ATOM PERCENT OF AL COMPLETELY SUPPRESSES THE DELTA PRIME PHASE. (REF: ELLINGER, LOS ALAMOS)
2. AT 10% AL THE PHASE $PuAl_2$ CANNOT BE REMOVED (EQUILIBRATED) EVEN AFTER HEAT TREATMENT FOR EXTENDED PERIODS BELOW 350° C. (REF: ELLINGER, LOS ALAMOS)
3. DIAGRAM BASED ON INFORMATION OBTAINED ON JUNE 20, 1960, FROM F. H. ELLINGER OF LOS ALAMOS SCIENTIFIC LABORATORY.

Fig. 6. Phase Diagram of Plutonium-Aluminum System

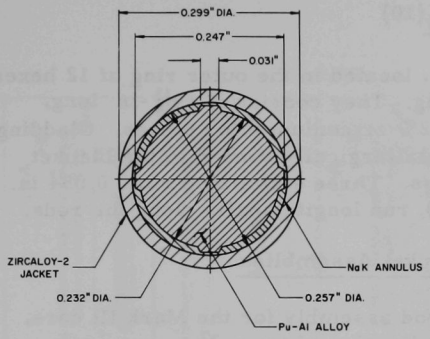

ID-103-1424

Fig. 7.

Cross Section through Mark IV Fuel Rod

A 0.0125-in. NaK-filled annulus between the slugs and jackets serves as a heat-transfer bond. A gas reservoir at the top of the upper blanket section serves to accommodate the thermal expansion of NaK and to provide for the accumulation of rare gas fission products. A Zircaloy-2 transition section is welded to the upper end of the tubular jacket. Threads on the upper portion of the transition section engage Type 304 stainless-steel rod handles, which are used for manual manipulation and for radiation shielding. To reduce flow resistance, the region of the rod handles between the transition section and the outlet plenum is reduced in cross section. At the bottom of each jacket is a Zircaloy-2, triangular-shaped tip designed for locating and orientating the fuel rods in a hexagonal grid.

3. Mark IV Core Blanket Rods

All Mark IV blanket rods are identical with fuel rods, with the exception that blanket material is substituted for fuel. Four slugs of depleted uranium, one 7.745 in., two 4.247 in., and one, 3.522 in. in length (all 0.235 in. in diameter), constitute the active section of the blanket. Such rods were needed to fill in the region between the fuel and the outer ring of M-3 blanket assemblies.

4. Thermocouple Rods

Special fuel and blanket rods were used to accommodate thermocouples for monitoring temperatures in the inner subassemblies. Sheath-type thermocouples were led through thimbles running downward through the handles, blanket, and fuel to an elevation corresponding to the centerline of the core. With the exception of the 0.086-in.-diameter thimbles, thermocouple rods are identical in all other respects with the respective fuel and blanket rods. Coolant temperatures were monitored with thermocouples inserted through special rod handles.

5. Radial Inner Blanket Rods[10]

The Mark III blanket rods, located in the outer ring of 12 hexes, were again used in the Mark IV loading. They consist of $19\frac{13}{16}$-in. long, 0.364-in.-diameter, natural uranium-2% zirconium alloy pieces. Cladding consists of 0.020 in. of Zircaloy-2 metallurgically bonded to the blanket material through a coextrusion process. Three stabilizing ribs, 0.054 in. in diameter (later ground to 0.046 in.), run longitudinally along the rods.

6. Fuel and Inner Radial Blanket Assemblies

A typical fuel or blanket rod assembly for the Mark III core, shown in Fig. 8, consists of a hexagonally-shaped tube, $2\frac{7}{8}$ in. across the flats, with a wall thickness of 0.040 in. At the bottom of the tube is a nozzle which fairs the hexagonal shape to that of a cylinder. Resting on the nozzle is a hexagonal grid perforated with circular and triangular holes. Figure 9 indicates the arrangement for the Mark IV core. The triangular holes receive the rod tips, which, in turn, locate and orient the rods. The round holes permit NaK to pass through the grid into the interstices between rods.

The set of holes approximately 3 ft above the lower support plate permits NaK to flow from the fuel assemblies into an outlet plenum chamber. The upper set of holes is for overflow.

The blanket assemblies differ from fuel assemblies in the following respects. Whereas fuel assemblies are designed to accept long-handled fuel and blanket rods, the blanket assemblies are designed to receive short-handled blanket rods only. Furthermore, blanket assemblies contain a set of holes located immediately below the seal plate to admit coolant in series flow. While these holes serve as an inlet for series flow, they also serve as an outlet for parallel-flow conditions. A seal plate in each blanket assembly separates inlet and outlet plenum chambers and serves to prevent short-circuit flow.

7. Rod Arrangement

A single Mark III radial inner blanket assembly contains 37 rod positions, 36 normally occupied with blanket rods and the 37th occupied by a centrally-located, expandable tightening rod, which forces the rods outward against the hex wall. A tightening rod, shown in Fig. 10, consists essentially of an outer split-tube which is expanded by means of a series of Woodruff key-type wedges riding in slots in the center shaft. The expansion is actuated by means of a nut-and-thread arrangement at the top of the tightening rod.

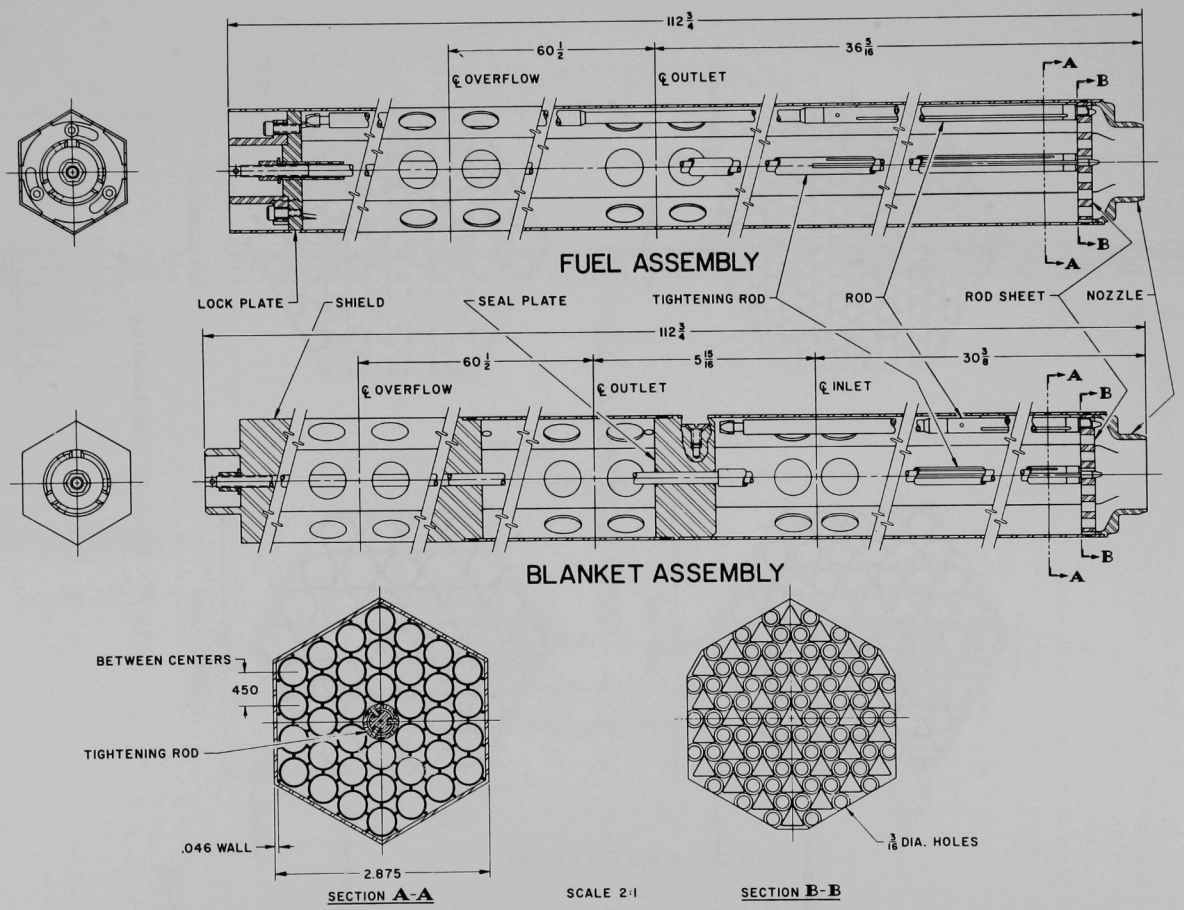

106-4051

Fig. 8. Mark III Fuel Assembly

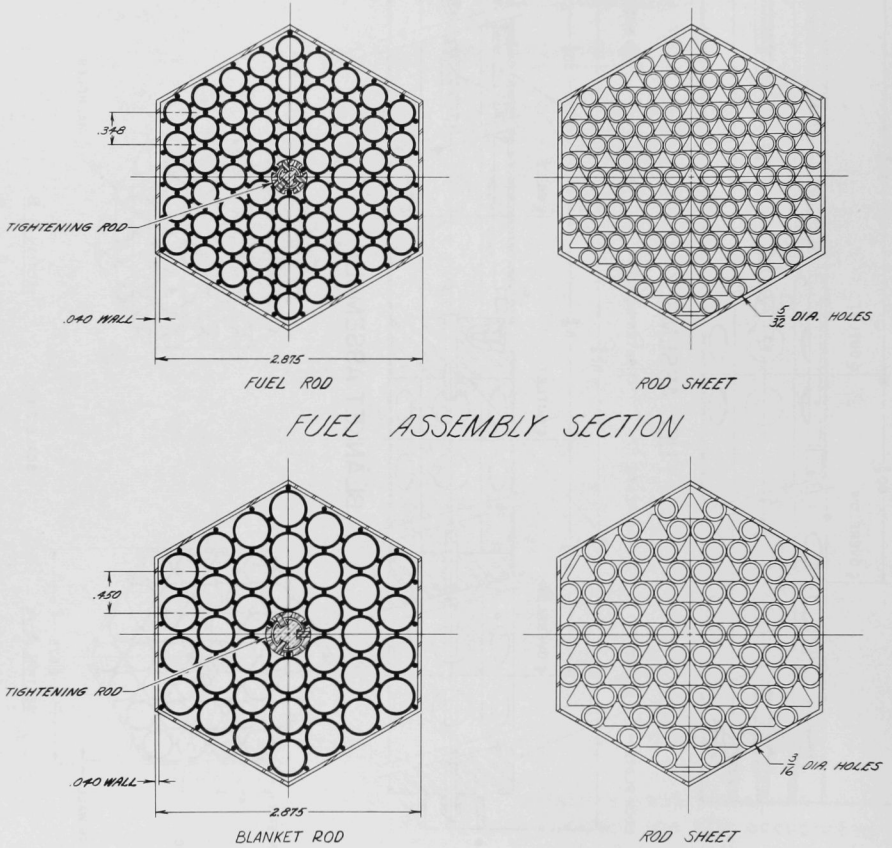

103-408

Fig. 9. Mark IV Hex Loading

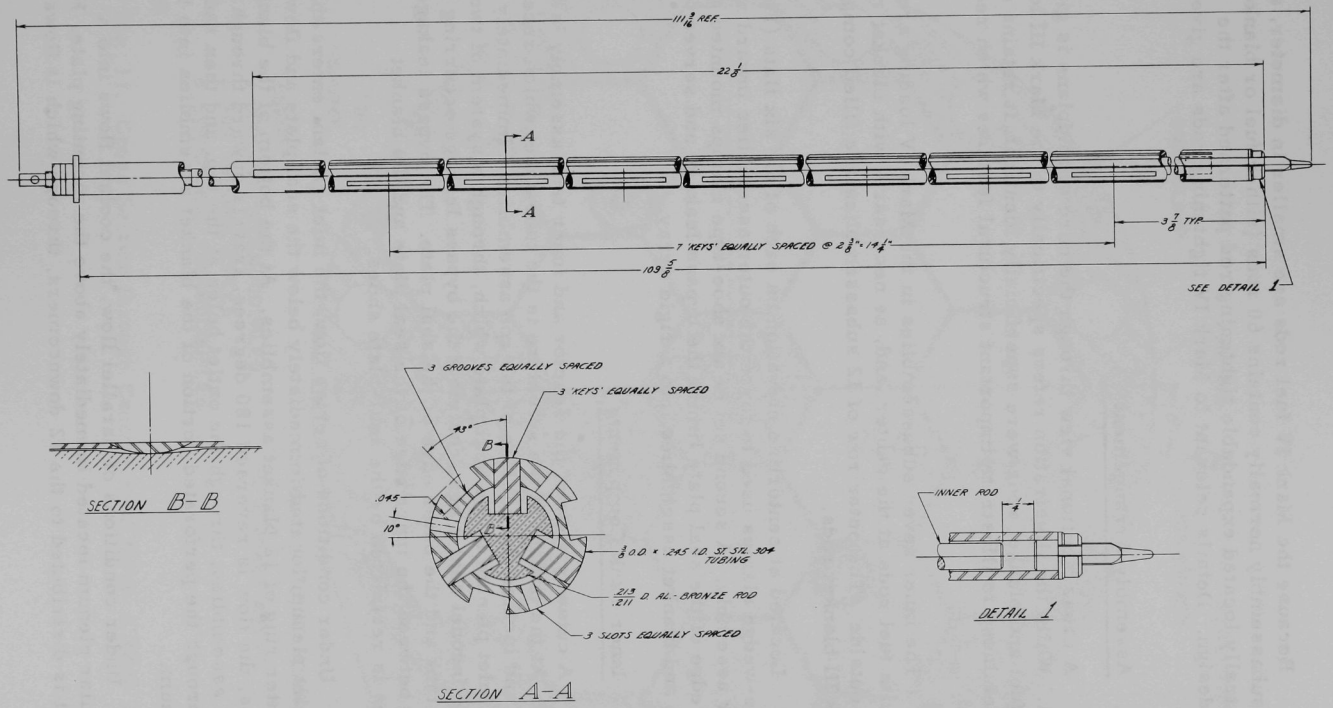

103-426

Fig. 10. Mark IV Tightening Rod

Because the Mark IV fuel rods are smaller in diameter, a Mark IV subassembly normally contains 60 rods (either fuel or blanket) and a centrally located expandable tightening rod patterned after the Mark III design. Details relevant to Mark IV tightening rods are given in Fig. 10.

8. Assembly Arrangement

A cross-sectional view through the core at midplane is given in Fig. 11. While the illustration refers specifically to the Mark III loading in which fuel and blanket rods were superficially identical, it retains sufficient usefulness to illustrate important structural features which remain unchanged.

The inner seven subassemblies in the Mark IV loading are filled, in part, with fuel rods at the center, and, as necessary, with blanket rods along the outside. The outer row of 12 subassemblies are filled completely with Mark III blanket rods.

Located at centerline elevation on each of the six flats (Fig. 11) are double-wedge clamps used to force the outer assemblies inward against the center assembly. A second set of six shoe-type clamps mounted along the inner edge of the seal plate limits the bypass leakage and serves to force fuel and blanket assemblies into a rigid array.

9. Inner Tank Components

A cutaway view of the reactor and inner tank assembly is shown in Fig. 12. At the bottom of the structure is the tube sheet which receives, supports, and locates the nozzles of the rod assemblies. Immediately above the inlet plenum is the seal plate which, through a system of two expandable Inconel seal rings, restricts the bypass leakage occurring between the tank and the outer edge of the seal plate. The bypass leakage occurring between the inner edge of the seal plate and the blanket assemblies is restricted by the seal-plate shoes.

Under conditions of series flow, the inlet coolant enters the annular inlet plenum located immediately below the seal plate and flows into the outer ring of 12 blanket assemblies. At the bottom of the blanket assemblies, the flow is reversed 180 degrees, travels upward through the seven fuel assemblies, through the outlet holes at the top, and then radially outward through the perforated portion of the blanket assemblies into the outlet plenum.

Under conditions of parallel flow, the coolant flows into a lower annular plenum located immediately above the mounting plate. Here the coolant is distributed to the 12 downcomers, through which it flows to

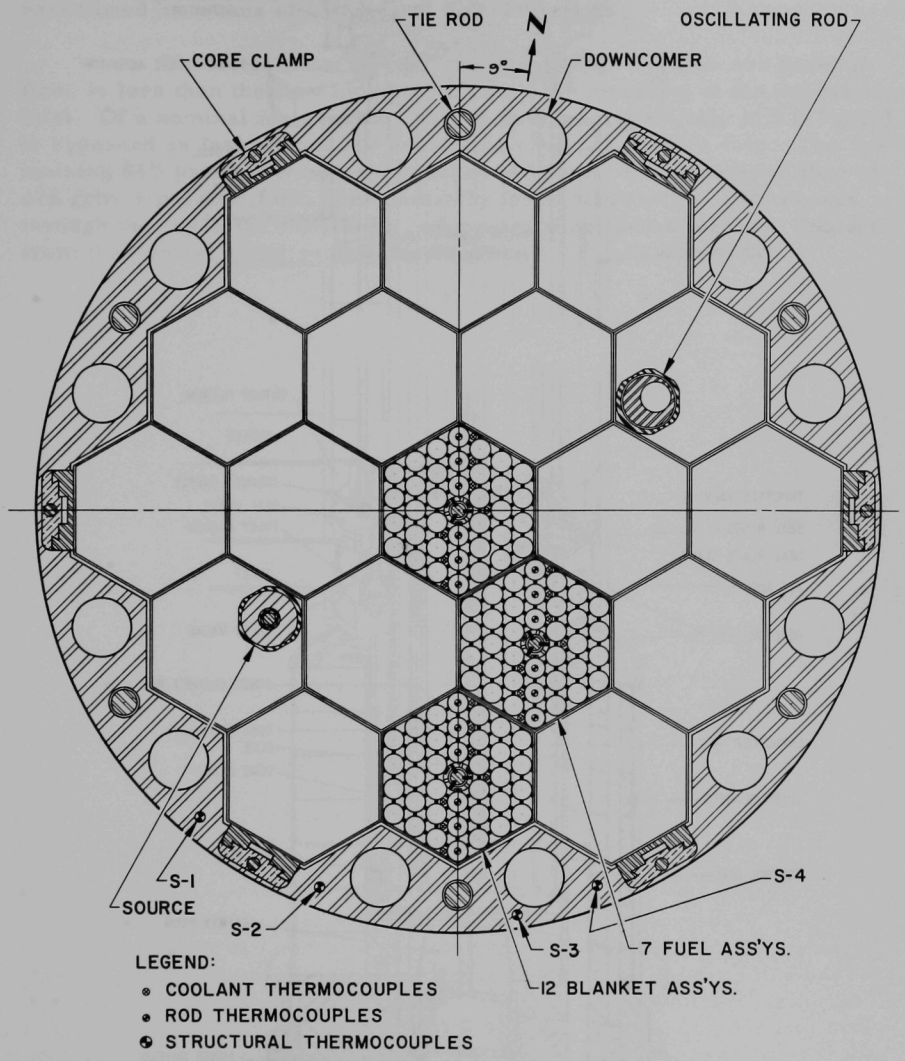

Fig. 11. Cross Section through Centerline of Core, EBR-I, Mark III

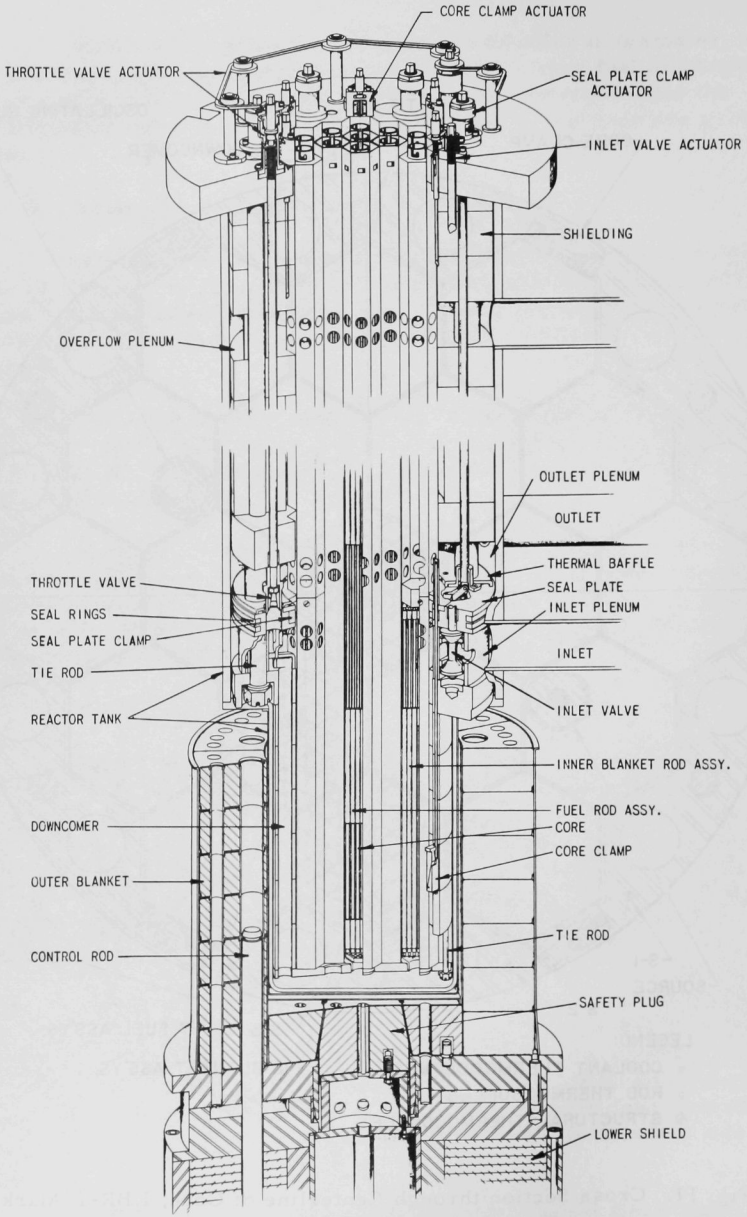

Fig. 12. Inner Tank Assembly, EBR-I, Mark IV

the lower plenum. Upward flow through fuel and blanket assemblies is partitioned by means of a series of throttle valves.

The actual flow through the core, both in series and parallel flow, is less than the flow indicated through the metering of the primary inlet. Of a nominal metered flow of 290 gpm, approximately 16% (47 gpm) is bypassed as leakage and for seal-plate cooling in series flow. The remaining 84% passes through the blanket and core. For a metered flow of 278 gpm in parallel flow, approximately the same fraction, 84%, passes through the core; the remaining 16% passes through the blanket. Coolant from the blanket outlet cools the seal plate.

III. THE CRITICAL LOADING

A. Neutron Source

The neutron source consisted of an activated antimony rod, surrounded by a beryllium thimble. As shown in Fig. 11, the source was located at the inner apex of one of the blanket assemblies. The accomodation of the source assembly required the removal of seven blanket rods.

The antimony rod was irradiated for 21 days at an average flux level of 2.94×10^{14} neutrons/cm^2 sec in the MTR. Calculations, based on thermal neutron-absorption cross-section data, resulted in an initial source strength of 5.7×10^{10} neutrons/sec as of Nov. 27, 1961. Subsequent decay of the Sb^{124} reduced the activity to a value of 9.7×10^8 neutrons/sec at the beginning (Nov. 21, 1962) of the critical experiments. To a minor extent, the neutron source strength was augmented by neutrons emitted by spontaneous fission in the Pu^{240} content of the fuel. Based on a value of 1.0×10^3 neutrons/sec-gram of Pu^{240} and an eventual loading of 1.46 kg of Pu^{240}, the contribution from this source amounted to only 1.5×10^6 neutrons/sec (0.15% of the antimony-beryllium source strength). Accordingly, corrections for neutrons liberated in the spontaneous fission of Pu^{240} were not applied to the subcritical data.

B. Instruments

The normal complement of flux monitoring equipment, described elsewhere,(14) was supplemented by five additional channels of information. Information pertinent to these additional channels is summarized in Table II.

Table II

SUPPLEMENT FLUX MONITORING FOR CRITICAL EXPERIMENTS

Channel	Detector	Filling Gas	Location	Loading	Voltage, volts
1	Westinghouse Fission		East Vertical Graphite Hole	1 g U^{235}	1900
2	1/2-in. gas-flow Fission	A-2% N_2	Blanket Hex L	4 mg U^{235}	300
3	1/2-in. gas-filled Fission	A-2% N_2	Blanket Hex J	6 mg U^{235}	300
A	Nancy Wood BF_3	$B^{10}F_3$	North-east Vertical Graphite Hole	30 cm pressure $B^{10}F_3$	1500
B	Nancy Wood BF_3	$B^{10}F_3$	North-west Vertical Graphite Hole	30 cm pressure $B^{10}F_3$	1550

Channel	Initial Elevation below Reactor Top, in.	Distance from Core Centerline
1	108	36 in. above
2	144	At core center
3	144	At core center
A	138	6 in. above
B	142	2 in. above

Nuclear information gathered from each channel described in Table II was readable from scaling equipment in the control room. To provide a continuous record of neutron level during loading operations, the signal from the Westinghouse fission chamber (Channel 1) was fed to a recording count-rate meter. An audio-indication of the counting rate, clearly audible to all operating personnel, was provided by a loud-speaker system coupled to the Channel 1 scaling equipment.

C. Fuel Loading Operations

The condition of the core, immediately before the loading of fuel, is as follows: an outer ring of 12 hexes filled to capacity with Mark III blanket rods, an inner ring of six assemblies filled with dummy rods and Mark IV blanket rods, and a central void created by the removal of the central hex. To simplify loading operations, all dummy rods (approximately 30 to a hex) were located along the inner periphery.

All loading operations were conducted with the lead cup in its lowermost position. While this procedure provided no shutdown margin, the probability of achieving criticality with the cup down was considered incredible because of the high shutdown worth of the cup and because incremental measurements were taken at intervals after raising the cup.

D. Approach to Critical

The first loading consisted of 60 fuel rods preloaded in the central hex (Channel A). The entire assembly was lifted with the overhead crane and inserted in 6-in. increments into position. Subcritical counts with all five channels were taken immediately following each incremental insertion. Counting results for this and all succeeding loadings are summarized for each channel in Tables III through VII. In all cases, corrections for the decay of the antimony source during the 9 days of subcritical measurements have been applied to the data tabulated. In accordance with established operational procedures, subcritical counts were repeated each morning for the last loading of the previous day. On certain occasions, near the end of the subcritical experiments, excessive counting rates necessitated the partial withdrawal of detectors. The continuity of data given in Tables III through VII reflect the application of normalization factors established with the detector(s) in the initial and final positions.

Subcritical counting data were taken with the cup in the following positions: fully down, 5.15 in. from the top of traverse, and fully up. In all cases, all safety and control rods were fully inserted.

The approach to criticality was guided primarily by information from Channels 1, A, and B. Little useful information was obtained from the two in-core fission chambers (Channels 2 and 3), primarily because of their low fissionable-material content.

Table III

SUBCRITICAL COUNTING DATA, CHANNEL 1

Loading	No. of Rods	Cup Down		Cup at 5.15 in.		Cup Up	
		cpm	1/cpm	cpm	1/cpm	cpm	1/cpm
No fuel	0	294	341×10^{-5}	422	237×10^{-5}	284	352×10^{-5}
1	60	527	190	674	148	514	195
2	102	862	116	1080	92.6	845	118
Repeat		841	119	1036	96.5	757	132
3	144	1300	76.9	1599	62.6	1531	65.3
4	186	1864	53.6	2872	34.8	2440	41.0
Repeat		1996	50.1	2692	37.1	2276	43.9
Repeat		1882	53.1	-	-	1938	51.6
5	228	3172	31.5	4196	23.8	3396	29.4
6	252	3978	25.1	5836	17.1	4847	20.6
Repeat		3407	29.4	5376	18.6	4632	21.6
7	276	5159	19.4	8672	11.5	7955	12.6
8	294	7032	14.2	13648	7.32	13720	7.29
9	312	9564	10.5	25722	3.89	36372	2.75
Repeat		8014	12.5	22564	4.43	32527	3.07
10	320	10217	9.79	35491	2.82	88904	1.12
11	327	11867	8.43	61326	1.63	-	-

Table IV

SUBCRITICAL COUNTING DATA, CHANNEL 2

Loading	No. of Rods	Cup Down		Cup at 5.15 in.		Cup Up	
		cpm	1/cpm	cpm	1/cpm	cpm	1/cpm
5	228	-	-	79	12.7×10^{-3}	88	11.4×10^{-3}
6	252	-	-	172	5.81	146	6.85
Repeat		71	14.1×10^{-3}	104	9.62	108	9.26
7	276	108	9.26	166	6.02	176	5.68
Repeat		158	6.33	142	7.04	-	-
8	294	199	5.02	231	4.33	345	2.90
9	312	172	5.81	428	2.34	810	1.23
Repeat		142	7.04	384	2.60	757	1.33
10	320	190	5.26	564	1.77	1882	0.531
11	327	239	4.18	985	1.02	-	-

Table V

SUBCRITICAL COUNTING DATA, CHANNEL 3

Loading	No. of Rods	Cup Down		Cup at 5.15 in.		Cup Up	
		cpm	1/cpm	cpm	1/cpm	cpm	1/cpm
9	312	58.5	17.1×10^{-3}	135	7.41×10^{-3}	255	3.92×10^{-3}
10	320	96.2	10.4	192	5.21	632	1.58
11	327	-	-	392	2.55	-	-

Table VI

SUBCRITICAL COUNTING DATA, CHANNEL A

Loading	No. of Rods	Cup Down		Cup at 5.15 in.		Cup Up	
		cpm	1/cpm	cpm	1/cpm	cpm	1/cpm
No fuel	0	15827	6.36×10^{-5}	7697	13.0×10^{-5}	4118	24.3×10^{-5}
1	60	22883	4.37	13580	7.36	8958	11.2
2	102	30478	3.28	19824	5.04	13910	7.19
Repeat		32309	3.10	21317	4.69	16544	6.04
3	144	42641	2.35	30076	3.32	21949	4.56
4	186	60909	1.64	46903	2.13	35845	2.79
Repeat		65559	1.53	50348	1.99	38972	2.56
Repeat		69489	1.44	-	-	40248	2.48
5	228	101072	0.99	86737	1.15	70551	1.42
6	252	136768	0.731	126699	0.79	107641	0.93
Repeat		136042	0.735	127751	0.78	108082	0.93
7	276	182968	0.547	194523	0.514	176246	0.567
8	294	238681	0.419	295932	0.338	296082	0.338
9	312	331063	0.302	562182	0.178	792508	0.126
Repeat		330024	0.303	561060	0.178	792423	0.126
10	320	382949	0.261	828784	0.121	1989613	0.0503
11	327	454223	0.220	-	-	-	-

Table VII

SUBCRITICAL COUNTING DATA, CHANNEL B

Loading	No. of Rods	Cup Down		Cup at 5.15 in.		Cup Up	
		cpm	1/cpm	cpm	1/cpm	cpm	1/cpm
No fuel	0	6257	16.1×10^{-5}	2696	37.1×10^{-5}	1396	71.6×10^{-5}
1	60	8340	12.0	4206	23.8	2653	37.7
2	102	10259	9.75	5738	17.4	3868	25.9
Repeat		10661	9.38	5990	16.7	-	-
3	144	13893	7.20	8460	11.8	6057	16.5
4	186	18516	5.40	12295	8.13	9340	10.7
Repeat		17946	5.57	11958	8.36	9027	11.1
Repeat		17975	5.56	-	-	9011	11.1
5	228	26818	3.73	19249	5.19	15610	6.41
6	252	32578	3.07	26754	3.74	22659	4.42
Repeat		32520	3.08	27259	3.67	23187	4.31
7	276	45105	2.22	42709	2.34	39016	2.56
8	294	57550	1.74	63364	1.58	64983	1.54
9	312	78379	1.28	119955	0.833	173788	0.575
Repeat		78066	1.28	118592	0.843	173140	0.575
10	320	90940	1.10	175101	0.571	427367	0.234
11	327	104884	0.953	294855	0.339	-	-

The various loadings are summarized in Table VIII, and the actual inverse counting rates for the three most reliable channels of information are presented graphically in Figs. 13 through 15. To avoid confusion, subcritical counting information for the 5.15-in. cup position has not been plotted. Figures 13 through 15 indicate that the critical mass estimates for Channels 1, A, and B amounted to 326 rods, a value in excellent agreement with the actual critical loading of 327 rods. Conservative estimates of the number of rods required for criticality with the cup down ranged from a low of 366 (Channel A) to a high of 381 (Channel 1). Since each value is based on a straight-line extrapolation of the inverse counting rate, a procedure that ignores the decrease in fuel worth as the radius becomes

larger, the smallest credible additional number of rods required for inadvertent criticality with the cup down is 39. Because rods were added in smaller and smaller increments as criticality approached, it is easy to understand why an overload sufficient to effect criticality with the cup down was considered incredible.

E. Corrections to the Critical Mass Value

To arrive at a more meaningful value for the critical mass, it is necessary to apply corrections for the position of control elements at criticality, and for the essentially empty thimbles in blanket hexes J and L. Subsequent calibration of the cup and control elements led to a value of 340 Ih supercriticality with the cup in its uppermost position. Replacement of the thimble in hex L with seven Mark III blanket rods resulted in a reactivity gain of 417 Ih. Hence, with both thimbles replaced by blanket rods, and with the cup in the uppermost position, the system would be supercritical by 1174 Ih, or 1.237% $\Delta k/k$ (based on 1% $\Delta k/k$ = 950 Ih). Conversion of the excess reactivity into mass units was made possible by the substitution of two Mark IV blanket rods by two fuel rods at the core blanket interface. Each substitution amounted to a gain of 112 Ih. Accordingly, the removal of 1174 Ih from the system corresponds to the replacement of 1174/112 or 10.5 fuel rods with blanket rods. The adjusted critical loading is then 316.5 rods or 27.789 kg of plutonium (all isotopes). Assuming an isotopic content of 94.4% (from Table VIII) the cold, clean, critical mass for Pu^{239} is 26.232 kg. Considering calculational uncertainties, the value of 27.8 kg (all isotopes) is in fair agreement with the value of 31.5 kg calculated by Baker.[17]

Table VIII

SUMMARY OF SUBCRITICAL LOADINGS

Loading No.	Date	No. of Rods	Total Pu, All Isotopes, kg	Total Pu^{239}, kg
1	11/20/62	60	5.241	4.953
2	11/20/62	102	8.937	8.453
3	11/21/62	144	12.632	11.941
4	11/21/62	186	16.332	15.438
5	11/23/62	228	20.029	18.928
6	11/23/62	252	22.136	20.924
7	11/26/62	276	24.239	22.914
8	11/26/62	294	25.818	24.406
9	11/26/62	312	27.404	25.899
10	11/27/62	320	28.099	26.548
11	11/27/62	327	28.715*	27.122*

*Critical at 15:00, 11/27/62.

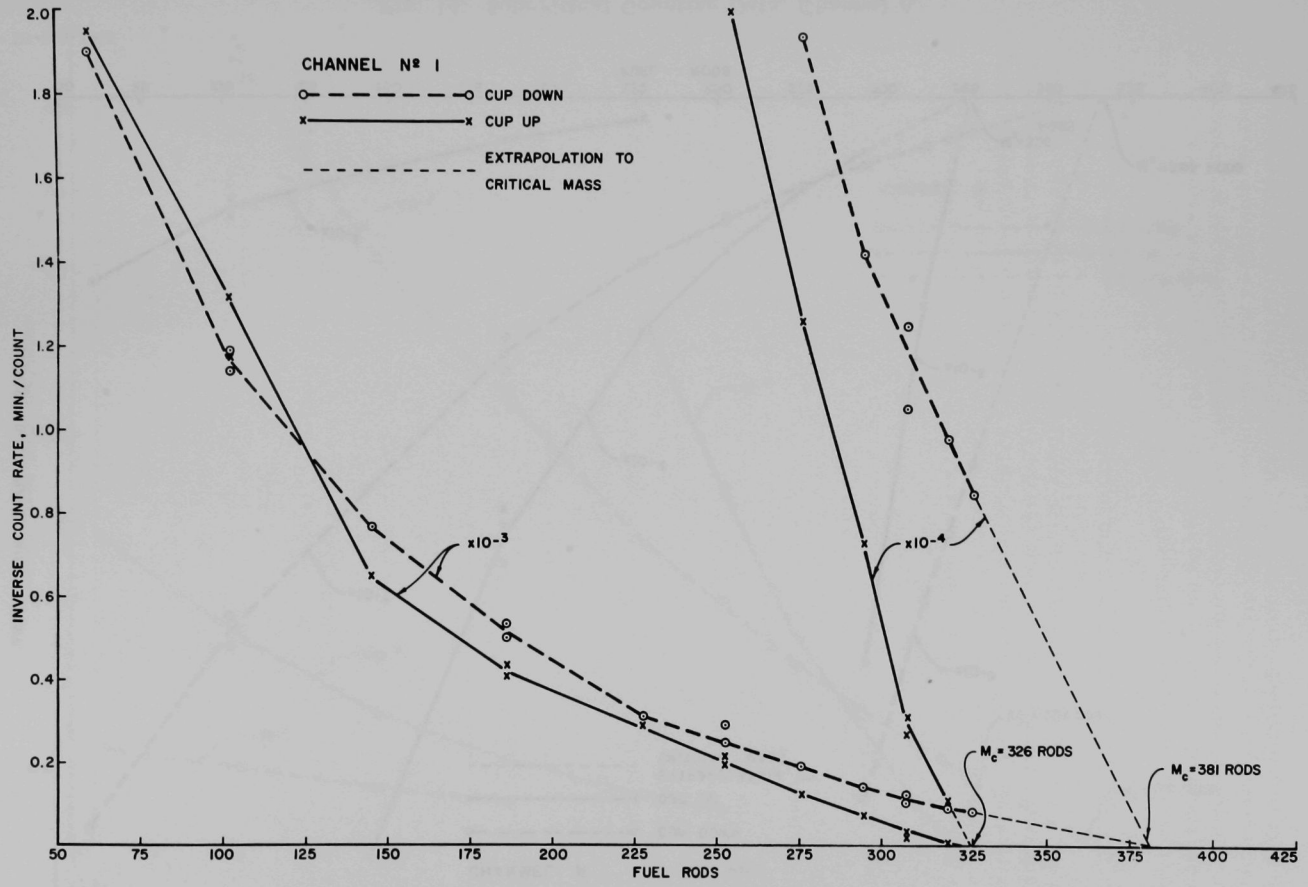

ID-103-1450

Fig. 13. Subcritical Counting Data, Channel 1

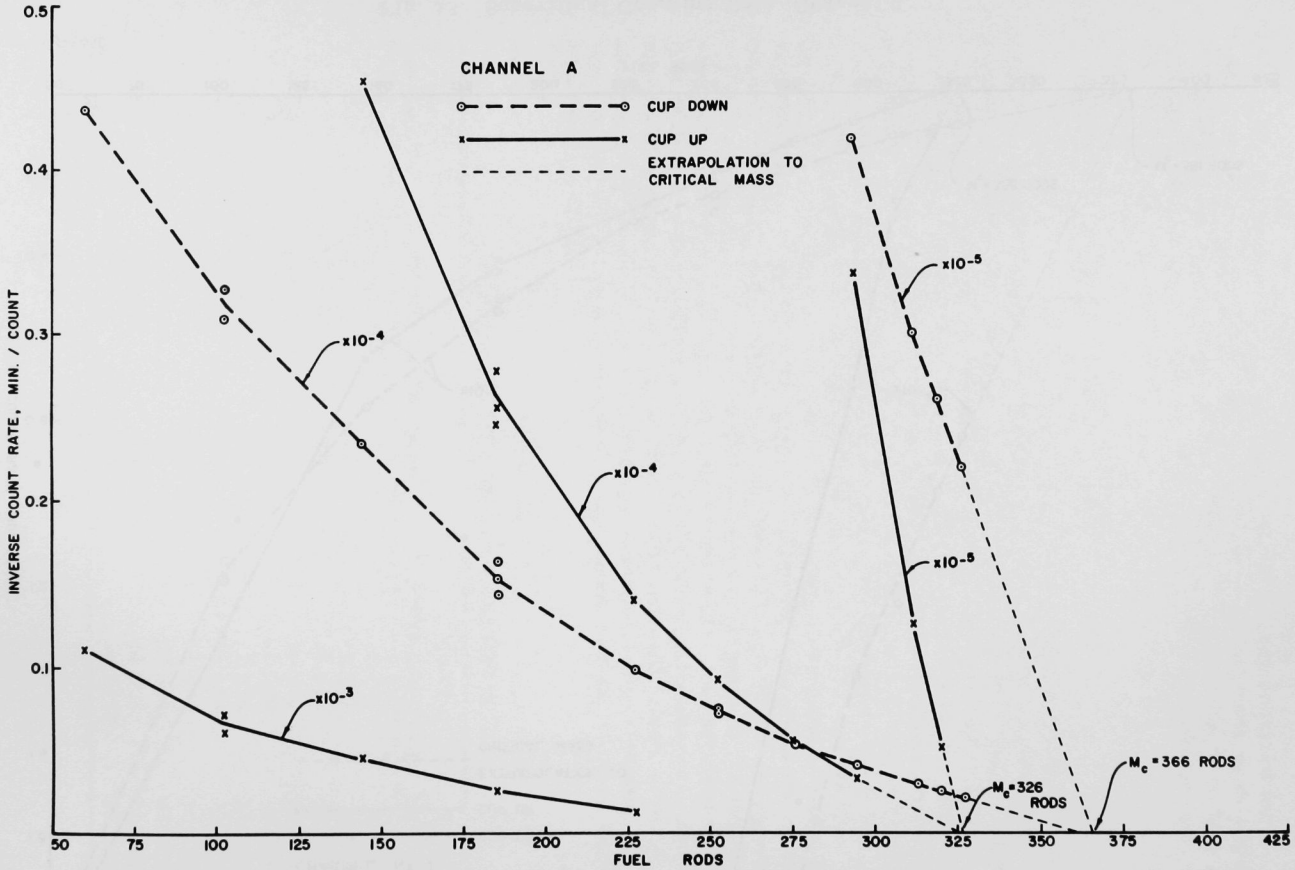

ID-103-1455

Fig. 14. Subcritical Counting Data, Channel A

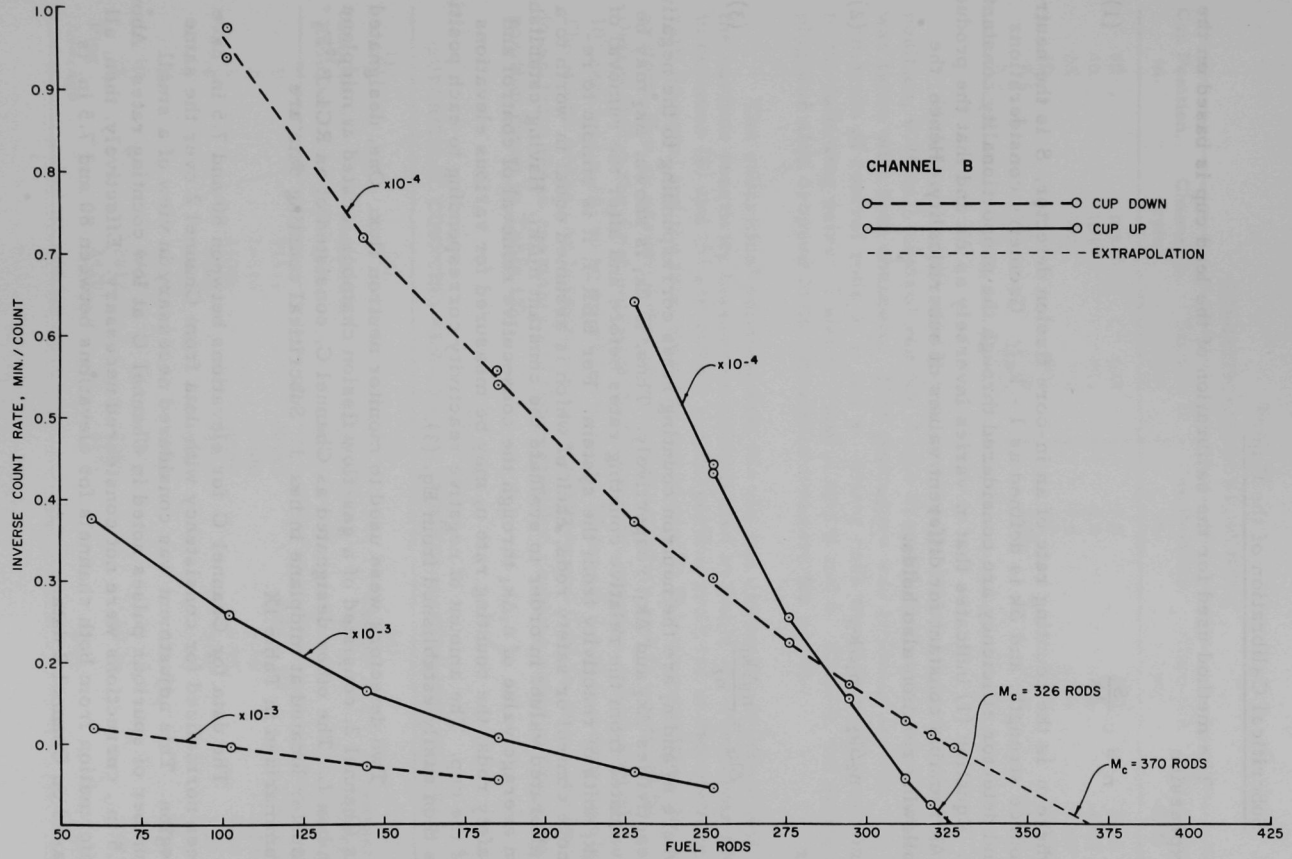

ID-103-1453

Fig. 15. Subcritical Counting Data, Channel B

F. Subcritical Calibration of the Cup

The method used for the calibration of the lead cup is based on the expression

$$n = c \frac{S}{\Delta k} \tag{1}$$

where n is the counting rate of an in-core fission detector, S is the neutron source strength, and Δk is defined as 1 - k_{eff}. Geometry considerations and detector efficiency are considered through the proportionality constant, c. Equation (1) indicates that n varies inversely as Δk and that the product $n\Delta k$ remains constant for different values of subcriticality. Hence, the following relation also holds:

$$n_2 \Delta k_2 = n_1 \Delta k_1, \tag{2}$$

or

$$\Delta k_2 = \frac{n_1 \Delta k_1}{n_2}, \tag{3}$$

where n_2 and n_1 are the neutron counting rates corresponding to the negative reactivities Δk_2 and Δk_1, respectively. Thus, if Δk_1 is known, Δk_2 may be evaluated from the relative counting rates before and after the removal of Δk_1 units of reactivity from the system. For EBR-I, it is simple to remove control or safety rods, each of which is assumed equal in worth to a calibrated value, in order to evaluate the constant $n_1 \Delta k_1$. Having established an average value of $n_1 \Delta k_1$ through the consecutive removal of control and safety rods, the counting rate n_2 may be measured for various elevations of the cup. The amount of negative reactivity corresponding to each position is then easily established from Eq. (3).

Two detectors were used to monitor neutron flux. One, designated as Channel 2, consisted of a gas-flow fission chamber located at midplane in hex L. The other designated as Channel C, consisted of an RCL $B^{10}F_3$ counter located at midplane in hex J. Subcritical counting data are summarized in Table IX.

The data for Channel C for elevations between 80 and 7.5 in. have been normalized for consistency with data from Channel 2 over the same region. This adjustment was considered necessary in view of a small number of spurious pulses noted in Channel C at low counting rates. Above 7.5 in., corrections were not considered necessary. Effectively, then, all information from both channels for elevations between 80 and 7.5 in. is based on Channel 2 data.

Table IX

SUBCRITICAL COUNTING DATA

Cup Position, in.	Channel 2, cpm	Channel C, cpm	Cup Position, in.	Channel 2, cpm	Channel C, cpm
80	185	618	5.0	868	3016
40	183	611	4.0	1276	4517
20	210	702	3.0	2138	7303
10	300	1001	2.0	4750	15508
7.5	469	1570	1.25	19745	63600
6.0	682	2161			

With the reactor subcritical at a cup position of 1.25 in. (critical position, 0.98 in.), control rod No. 2 was dropped and a subcritical count was taken with both channels. This procedure was repeated for the removals of control rods 3, 1, and 4. Safety rods were dropped according to the following pairs: 7 and 8, 1 and 2, and 5 and 6. Finally, the safety plug was also dropped in an attempt to measure its worth.

The subcritical counting data for the two channels corresponding to the various reactivity losses are summarized in Table X. The values given in columns (4) and (5) are simply the respective products of the counting rate (in cpm) and the total negative reactivity (in Ih) removed from the system, if it is assumed that one control or safety rod is worth 30 Ih. Disregarding the first entry for both channels, average values of 9.92×10^5 and 3.31×10^6 were found for $n_1\Delta k_1$ in Channels 2 and C, respectively. The worth of the cup between its down position and 0.98 in. may then be found from these constants and the respective counting rates at the down position given in Table IX.

Table X

SUBCRITICAL COUNTING RESULTS FOR CONTROL-SAFETY ROD REMOVAL

(1) Total No. of Rods Out	(2) Channel 2, cpm	(3) Channel C, cpm	(4) Channel 2, $n_1\Delta k_1$, cpm x Ih	(5) Channel C, $n_1\Delta k_1$, cpm x Ih
1	29571	95441	8.85×10^5	2.86×10^6
2	16130	53380	9.68	3.20
3	11066	36390	9.98	3.28
4	8184	27259	9.80	3.27
6	5529	18314	9.95	3.30
8	4139	13950	9.91	3.34
10	3337	10867	10.00	3.14
12	2812	10089	10.10	3.62
Plug	2420	8591		
Average			9.92	3.31

Hence, for Channel 2,

$$k_2 = \frac{n_1 k_1}{n_2} = \frac{9.92 \times 10^5}{185} = 5360 \text{ Ih};$$

and for Channel C,

$$k_2 = \frac{3.31 \times 10^6}{618} = 5360 \text{ Ih}.$$

The agreement between the values for the two channels is not surprising, since the cup down data for Channel C are based, in part, on a cross-normalization of data for elevations below 7.5 in. The normalization by itself, however, cannot account for the exact agreement; this must be regarded as fortuitous.

A subsequent cup calibration (through period measurements) between 0.98 in. (the critical position) and the fully-up position resulted in a value of 168 Ih for the reactivity worth. Hence, the entire travel of the cup between the fully-down position (80 in.) and the fully-up position (0.00 in.) amounts to 5360 + 168, or 5528 Ih. If it is assumed that 950 Ih = 1% $\Delta k/k$, the equivalent value in reactivity units becomes 5.82% $\Delta k/k$.

The cup worth as a function of elevation between the fully-down and fully-up positions is summarized in Table XI. Allowance has been made for the worth between 0.98 and 0.00 in. The reactivity worth of the cup

Table XI

CUP WORTH AS A FUNCTION OF ELEVATION*

	Cup Worth, Channel 2		Cup Worth, Channel C	
Cup Elevation, in.	Inhours	% $\Delta k/k$	Inhours	% $\Delta k/k$
80	5528	5.82	5528	5.82
40	5592	5.89	5598	5.89
20	4898	5.16	4898	5.16
10	3478	3.66	3478	3.66
7.5	2288	2.41	2278	2.40
6.0	1718	1.70	1798	1.89
5.0	1313	1.38	1278	1.35
4.0	948	1.00	959	0.95
3.0	633	0.67	622	0.65
2.0	357	0.38	382	0.40
1.25	218	0.23	220	0.23
0.00	0	0.00	0	0.00

*Uranium Cup.

between the fully-up and fully-down positions is plotted in Fig. 16. The same information for the region 0 to 7.5 in. is expanded in Fig. 17. The worth of the uranium safety plug can also be roughly estimated from the data given. Using the data from Channel 2, the more reliable at low counting rates, a value of 51 Ih or 0.054% $\Delta k/k$ was established.

Period measurements were eventually used to reestablish the cup worth over the region 0-4.5 in. The results are given in Fig. 18. A comparison of these results with those obtained through subcritical measurements (Fig. 17) reveals that the two sets of data are consistent within the limits of ±25 Ih.

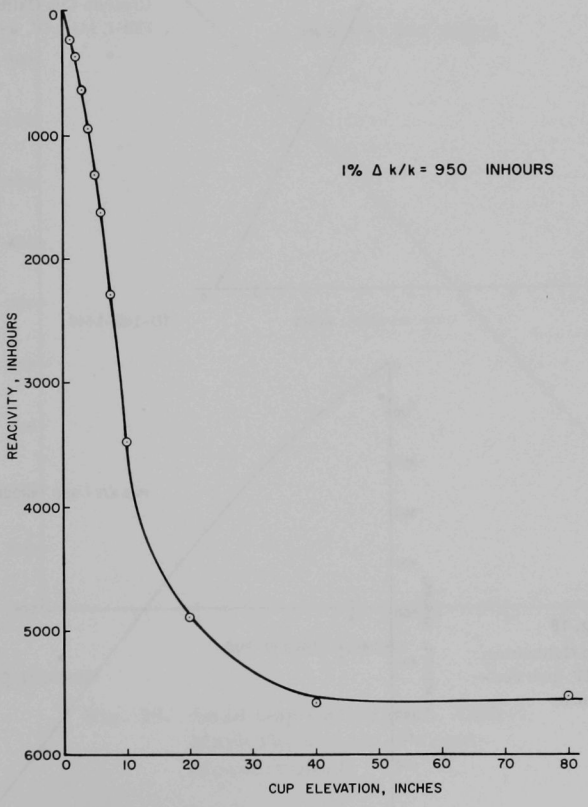

ID-103-1449

Fig. 16. Uranium Cup Calibration, EBR-I, Mark IV, 0-80 in.

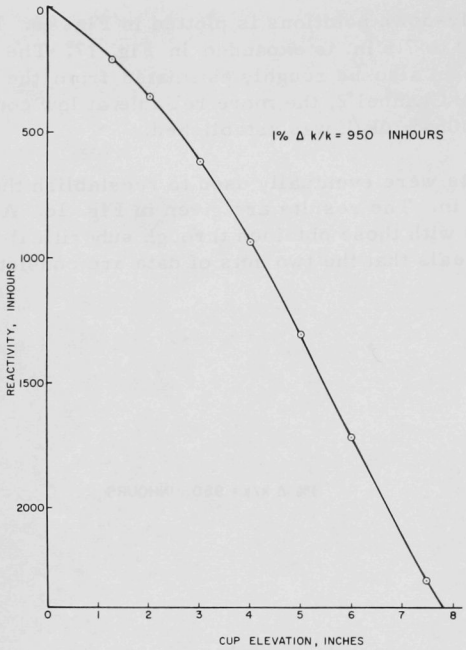

Fig. 17
Uranium Cup Calibration
EBR-I, Mark IV, 0-7.5 in.

ID-103-1446

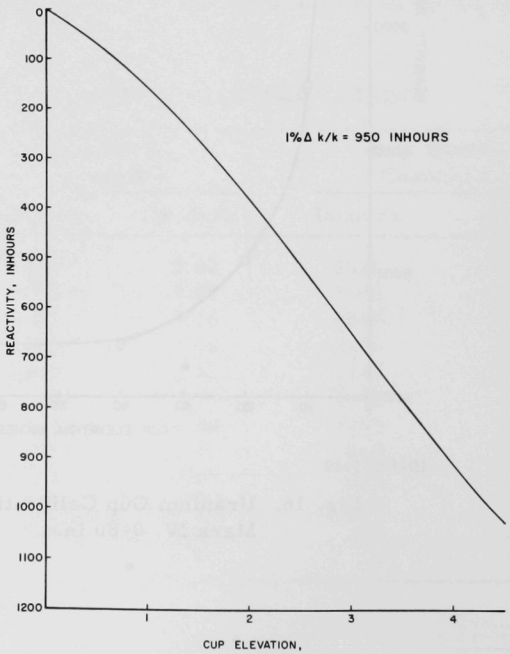

Fig. 18
Uranium Cup Calibration,
EBR-I, Mark IV, from Peri-
od Measurements

ID-103-1454

Eventually, it was necessary to remove the uranium cup and substitute in its place an essentially-identical cup filled with lead. The results of a calibration based on period measurements are presented in Fig. 19. A comparison of the relative uranium and lead cup worths at 3.00 in. reveals that the worth of the lead cup is greater than that of its uranium counterpart by the factor 1.19.

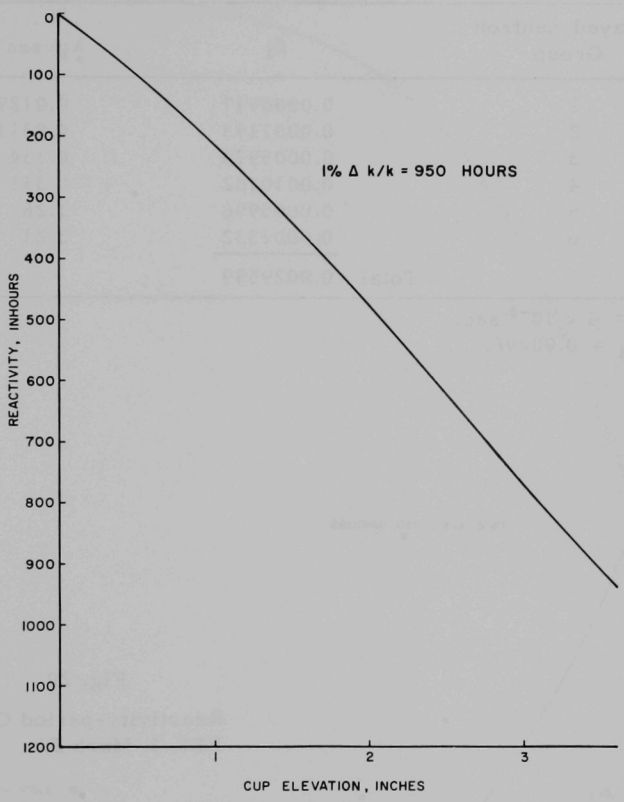

ID-103-1458

Fig. 19. Lead Cup Calibration, EBR-I, Mark IV, 0-3 in., Period Measurement

G. Calibration of Control Rods

The relationship between period and reactivity (in inhours) was established through the basic inhour equation using the delayed-neutron

parameters listed in Table XII. The results, illustrated graphically in Fig. 20, may be used to estimate the reactor period resulting from a given reactivity insertion in inhours.

Table XII

DELAYED-NEUTRON PARAMETERS

Delayed-neutron Group	β_i	λ_i, sec^{-1}
1	0.0000917	0.0129
2	0.0007193	0.0311
3	0.0005979	0.134
4	0.0010182	0.331
5	0.0003996	1.26
6	0.0001332	3.21
Total	0.0029599	

$l^* = 4 \times 10^{-8}$ sec.
$\beta_{eff} = 0.00296$.

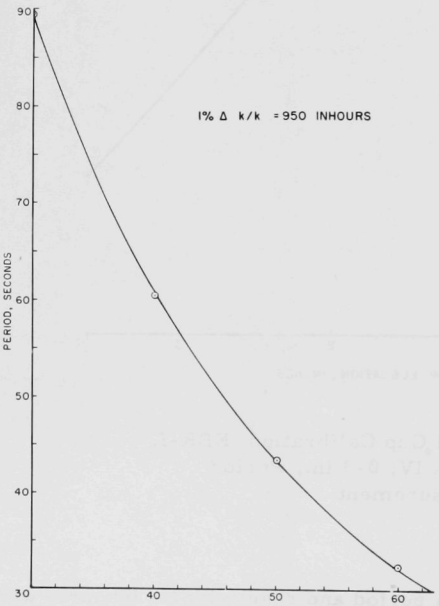

ID-103-1445

Fig. 20

Reactivity-period Curve, EBR-I, Mark IV

A typical control-rod calibration curve, based on period-reactivity information, is shown in Fig. 21. Since all control and safety rods are symmetrically located in the lead reflector, the calibration curve of Fig. 21 holds for all 12 safety or control rods.

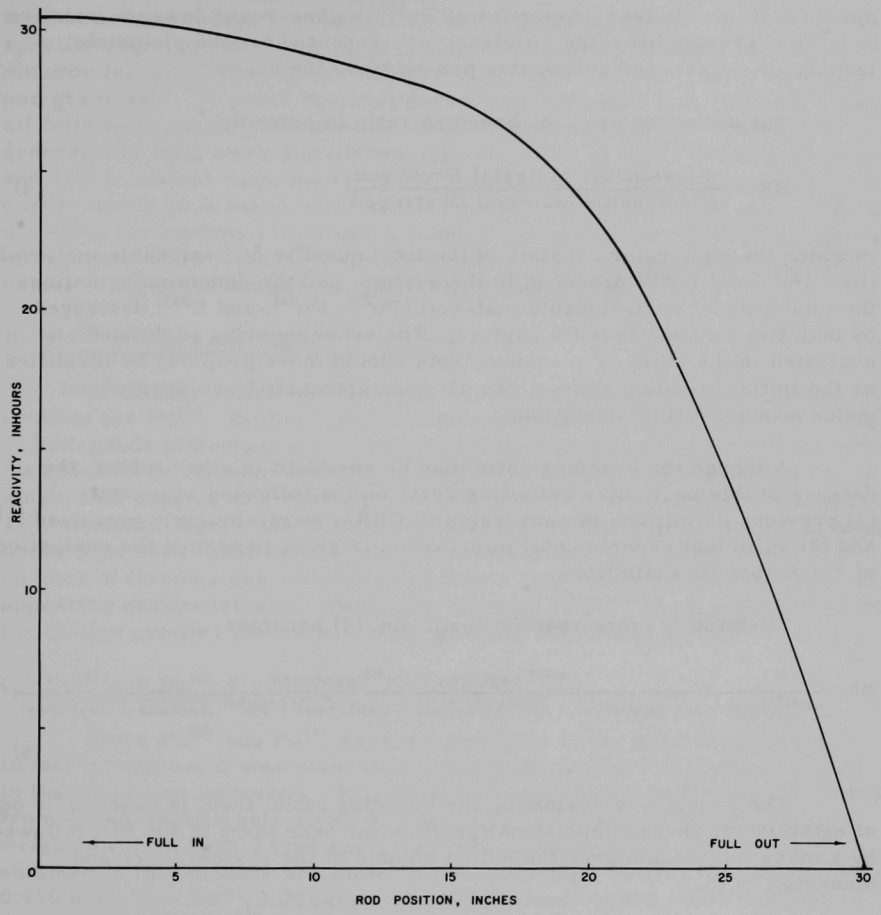

ID-103-1460

Fig. 21. Control-rod Calibration, EBR-I, Mark IV, Lead Cup

IV. BREEDING GAIN MEASUREMENTS

The plutonium loading in EBR-I provided an excellent opportunity to compare the relative breeding merits of U^{235}- and Pu^{239}-fueled systems of essentially the same size and structural composition. In view of the more favorable nuclear properties of Pu^{239} (higher ν and lower α, relative to U^{235}), a greater breeding efficiency was expected for the plutonium loading. As discussed below, this proved to be the case.

The definition used for breeding ratio is given by

$$BR = \frac{\text{Fissionable Material Produced}}{\text{Fissionable Material Destroyed}}, \tag{4}$$

in which the numerator consists of the total quantity of fissionable material (i.e., Pu^{239} and Pu^{241}) produced in the system, and the denominator defines the total amount of fissionable material (Pu^{239}, Pu^{241}, and U^{235}) destroyed by both fission and parasitic capture. The breeding ratio so defined and evaluated in the Mark IV measurements should more properly be identified as the initial breeding ratio, since all measurements were carried out under nonequilibrium conditions.

Although the breeding ratio may be specified in other forms, the defense of this particular definition rests on the following arguments: (1) previous definitions of conversion in EBR-I were similarly premised,[18] and (2) sufficient experimental information is given to permit the evaluation of more specific definitions.

Restated in more specific form, Eq. (4) becomes

$$BR = \frac{U^{238}\text{ captures} + Pu^{240}\text{ captures}}{U^{235}(\text{fissions} + \text{captures}) + Pu^{239}(\text{fissions} + \text{captures}) + Pu^{241}(\text{fissions} + \text{captures})}. \tag{5}$$

The problem of evaluating the breeding ratio, then, is essentially one of establishing three-dimensional profiles for each term in Eq. (5), followed by a mass integration over the entire volume of the system (core and blankets).

A. U^{235} Fission and Capture Patterns

The specific U^{235} fission rate, defined as the number of U^{235} fissions per gram of U^{235}, was established indirectly from observations of the fission-product activity induced in enriched foils distributed at fixed locations throughout the various breeding blankets.[16] All observations were carried out with a precision pulse-height analyzer, fed by a 2 x 2-in. Harshaw Type S Integral Line Scintillator. As an arbitrary but fixed and reproducible

reference point, all events having energies greater than 662 keV (the photopeak of Cs^{140}-Ba^{140}) were registered and integrated. To eliminate the effects of power changes between runs and of radioactive decay, all counting observations were made relative to those carried out on a single enriched monitor foil, which was irradiated under identical conditions of power and time at a fixed reproducible position in the graphite region. Division of the specific counting rate for a given foil by the specific counting rate of the monitor foil gave directly the number of fissions-product events detected per gram-sec. To avoid spectral distortions and neutron-streaming effects, all foils were sandwiched between slugs of depleted uranium metal. In general, the foils were distributed approximately at 1-in. vertical increments and 1/2-in. radial increments. Such measurements resulted in a family of curves which gave the number of fissions per monitor fission as a function of radius for various elevations throughout the blankets. Parasitic capture effects in U^{235} (to form U^{236}) were estimated from the fission profiles and values of α_{25} given earlier for EBR-I by Kafalas et al.[19]

B. Pu^{239} Fission and Capture Patterns

A similar technique was used to evaluate the fission and capture profiles for Pu^{239}. In this case, the foils consisted of approximately 15 mg of fuel-grade plutonium encapsulated in thin aluminum jackets. Aluminum-clad fuel slugs approximately 1 in. long were used to separate the foils. A single foil, located at a reproducible position at core midcenter, was used as a monitor. Again, the results of the traverse measurements and counting operations were manifested in the form of a family of curves, giving the number of fissions per monitor fission as a function of radius, with elevation appearing parametrically. Parasitic captures in Pu^{239} were estimated from the fission profiles and values of α_{49} given by Kafalas et al.[19]

C. Pu^{240} and Pu^{241} Fissions and Captures

Since Pu^{240} and Pu^{241} were not available in the pure form in sufficient quantities, it was necessary to evaluate fission and capture effects in these species indirectly. Effective cross-section values were estimated from cross-section sets given in Yiftah et al.,[20] which, in turn, were weighted for an EBR-I type spectrum.[21] Fission cross-section values obtained in this manner amounted to the following: Pu^{239}, 1.81 barns; Pu^{240}, 0.950 barn; and Pu^{241}, 2.00 barns. Capture values, on the other hand, were estimated to be: Pu^{240}, 0.20 barn; and Pu^{241}, 0.20 barn. If it is assumed, as a first-order approximation, that the fission yields and effective fission-product half-lives are the same for fission in each of the three species, the specific fission rate was apportioned, according to cross section, between the various species.

D. U^{238} Capture Patterns

Capture patterns for U^{238} were evaluated indirectly through observations of the 106-keV photopeak of Np^{239} generated in depleted uranium foils distributed throughout the various blankets. The use of this approach presupposes the application of accurate corrections for the effects of fission products generated through threshold fission in U^{238}. The technique developed for the separation of the fission-product component, described in detail elsewhere,[16] is based on an experimental measurement of the ratio of fission-product activity in a fixed, high-energy band (where Np^{239} activity is missing) to that in a fixed, low-energy band, which effectively straddles the Np^{239} 106-keV photopeak.

An illustration of this concept is provided by Fig. 22, which gives the gamma spectrum associated with a depleted uranium foil which, in turn, had been irradiated in a hard neutron spectrum. One band, designated as A, includes the integrated response over the energy region 87 to 123 keV. The other band, designated as B, includes the integrated response of all events having energies greater than 662 keV. All events in Band B are the result of gamma transitions from fission products formed either by threshold

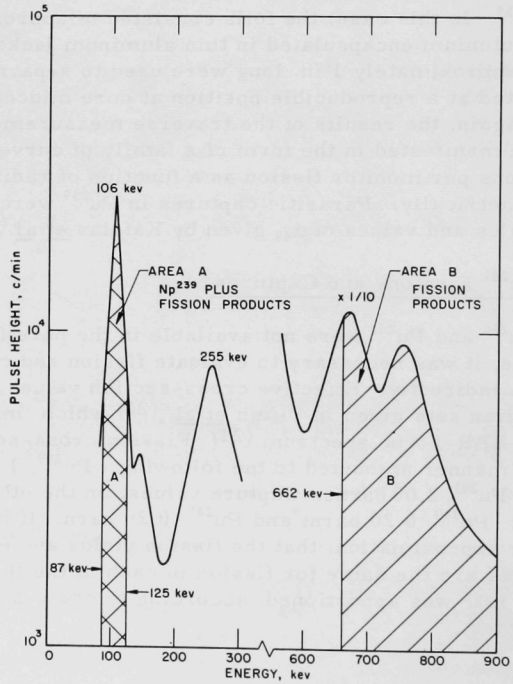

103-445

Fig. 22. Definition of Bands A and B

fission in U^{238} or by fast fission in a 0.22% contamination of U^{235}. Events falling in Band A, on the other hand, include the following components: (1) Np^{239} and Pu^{239} gammas and Pu^{239} K X-rays and (2) fission-product gammas and uranium K X-rays, the latter originating from the conversion of weak fission-product gammas in uranium. The first of these is specifically associated with the decay of Np^{239} and is, accordingly, the signal of interest. The second, a background component, is directly the result of fission-product activity.

To establish the ratio of fission-product activity in Band B to that in Band A, $(B/A)_{fp}$, measurements were carried out on radiochemically-separated samples of U^{238} and U^{235} fission products. The results demonstrated that for cooling periods longer than 35 hr, the ratio $(B/A)_{fp}$ measured for U^{238} was indistinguishable from that measured for U^{235}. With this fact established, similar measurements were conducted on a set of depleted and enriched foils that had been irradiated under identical conditions of time and neutron flux at the center of the core. Using the enriched foil data to correct for the effects of U^{235} fission products in the depleted foil, a curve giving the time dependence of $(B/A)_{fp}$ was established. Thus, for any given irradiated depleted foil and for any specified cooling period in excess of 35 hr, a simple measurement of the Band B response permits a direct evaluation of the Band A fission-product activity. Subtraction of this component from the gross Band A response yields the Np^{239} activity.

The reliability of the method was tested by following the half-life of the Np^{239} component in a foil that had been irradiated under extremely hard neutron-flux conditions at the center of the EBR-I core. Since the measured half-life was in excellent agreement with the commonly accepted value, it may be concluded that the method is satisfactory. The technique was particularly useful since hundreds of foils could be consecutively analyzed over a reasonable period of time, i.e., 6 to 12 hr.

E. U^{238} Fission Patterns

While the effects of fast (threshold) fission in U^{238} are not considered in the definition of breeding ratio [see Eq. (5)], a substantial fraction of the total fissions occurs in this species. Since no credit is taken for U^{238} fissions, the effects are manifested in the form of a bonus. The only extra information needed for an evaluation of this effect is a relative measurement of the number of fissions occurring in U^{238}. Such information was obtained indirectly by comparing the Band B counting rate for any given traverse foil with the Band B counting rate of the depleted monitor foil (located at the interface of the core and the upper blanket). A portion of the total fission-product activity generated in any given depleted foil arises through fission in the 0.22% content of U^{235}. For the most part, such effects were small and were satisfactorily estimated from information gathered in the enriched foil traverses. Such measurements resulted in a family of curves giving the number of U^{238} fissions per monitor fission as a function of radius, with elevation appearing parametrically.

F. Integration of Fission and Capture Patterns

To compare all traverse results on a common power-time basis, radiochemical analyses were conducted on a complete set of monitor foils, each of which had been irradiated simultaneously at the respective monitoring locations. Analyses for total fissions in the plutonium monitor foil were carried out by the ICPP Analytical Section of Phillips Petroleum Company.[22] Analyses for total fissions and captures in the depleted foil, and for total fissions in the enriched foil, were conducted by Argonne personnel at Argonne, Illinois.[23] A mass integration of the various fission and capture patterns over the volume of the system resulted in values for the total number of captures and fissions per monitor event. Multiplication by the respective value obtained from the radiochemical analyses gave directly the total number of fissions and captures for the various species. The results are summarized in Table XIII.

Table XIII

SUMMARY OF FISSIONS AND CAPTURES

Species	Fissions	Captures
U^{235}	0.1429×10^{18}	0.0362×10^{18}
Pu^{239}	0.9146×10^{18}	0.0841×10^{18}
Pu^{240}	0.0259×10^{18}	0.0055×10^{18}
Pu^{241}	0.0054×10^{18}	0.0005×10^{18}
U^{238}	0.251×10^{18}	1.492×10^{18}

Substitution of values from Table XIII into Eq. (5) results in a breeding ratio of 1.27 ± 0.08, where the precision limits have been established in a manner previously given in detail.[16]

G. Fast-fission Bonus

By defining the fast-fission bonus as the ratio of the number of fissions in fertile material to the number of absorptions in fissionable material, an evaluation of the fast-fission bonus may be obtained from the information of Table XIII and the following expression:

$$\text{FFB} = \frac{\text{Fissions in } U^{238} \text{ and } Pu^{240}}{\text{Fissions and Captures in } U^{235}, Pu^{239}, \text{ and } Pu^{241}}. \qquad (6)$$

Substitution of pertinent values into Eq. (6) results in a value of 0.23 for the fast-fission bonus. It follows, then, that for every 100 atoms of fuel material

destroyed, approximately 21 atoms of U^{238} and two atoms of Pu^{240} are fissioned. Such fissions contribute to the power produced and significantly improve the neutron economy.

H. Structural Absorption and Leakage

The inefficiency of breeding in the EBR-I system may be estimated by considering the basic neutron balance equation given by

BG = breeding gain

$$= \frac{X_1(\nu_1 - 1 - \alpha_1) + X_2(\nu_2 - 1 - \alpha_2) + X_3(\nu_3 - 1 - \alpha_3) + F_4(\nu_4 - 1) + F_5(\nu_5 - 1) - (A + L)}{X_1(1 + \alpha_1) + X_2(1 + \alpha_2) + X_3(1 + \alpha_3)}, \quad (7)$$

where X_1, X_2, and X_3 are the fission fractions for U^{235}, Pu^{239}, and Pu^{241}, respectively, and where F_4 and F_5 are, respectively, the fission fractions for U^{238} and Pu^{240}. The subscripts 1 through 5 refer, respectively, to U^{235}, Pu^{239}, Pu^{241}, U^{238}, and Pu^{240}. The number of neutrons "wasted" (i.e., unavailable for capture in U^{238} and Pu^{240}) is given by A + L, where A is the number of neutrons lost through capture in structural materials and coolant per fission, and L is the number of neutrons per fission leaking from the system. Hence, substitution of the experimental value of 1.27 for the breeding ratio into Eq. (7), along with appropriate values for ν and α, permits an evaluation of the combined absorption-leakage term, A + L. Information from Table XIII may be used to evaluate X_1, X_2, X_3, F_4, and F_5. Estimates of ν through α, based on information compiled by Okrent,[24] consist of the following: ν_1 (U^{235}), 2.50; ν_2 (Pu^{239}), 2.90; ν_3 (Pu^{241}), 2.99; ν_4 (U^{238}), 2.51; and ν_5 (Pu^{240}), 2.77. While at best approximate, values of 0.09 and 0.25, based on the work of Kafalas et al.,[19] were assumed for the ratio of capture to fission in Pu^{239} and U^{235}, respectively. Since information was not available for capture in Pu^{241}, a value of 0.10 for α_3 was arbitrarily assumed. Substitution of the various values into Eq. (7) results in a value of 0.66 for the combined leakage-absorption term, A + L.

If it is assumed that leakage and structural absorption effects are the same for all neutrons, irrespective of their origins, the significance of the above evaluation lies in the fact that approximately 0.66 neutron per weighted fissile absorption disappears through absorption processes in the structure and coolant and through leakage from the breeding blankets. In earlier conversion ratio measurements on a U^{235}-fueled EBR-I system, Kato[16] estimated a combined absorption-leakage value of 0.44. The difference between the earlier value and the value given above may be explained, in part, on the basis of strong differences in blanket volume fractions. In earlier loadings (i.e., Marks I and II), the uranium content of the outer radial blanket was 71 v/o. In the change from the Mark II to the Mark III loading (hence, Mark IV), the uranium content was reduced to 50%.

The change also effected an increase in values for the volume fractions of structural materials and coolant. From these considerations, it seems likely that the absorption and leakage terms (i.e., A and L) are larger for the Mark IV system, and that the difference between the values of 0.44 and 0.66 is real.

I. Axial and Radial Plots of Fission and Capture Events

The information gathered in the Mark IV breeding-gain measurements may be used to construct axial and radial plots of fission and, in certain instances, capture events for the various species. To permit a critical comparison between the various data, all events have been normalized to unity for Pu^{239} fissions at core midcenter. All intensities are given in terms of fissions or captures per gram of material.

A radial transverse for Pu^{239} and U^{235} fissions is given in Fig. 23. A slight extrapolation of the Pu^{239} fission data to the edge of the core results in a value of 1.50 for the center-to-edge fission ratio at centerline elevation. The relatively slow decrease in the specific U^{235} fission rate with increase in core radius reflects a softening of the neutron spectrum through elastic and inelastic scattering processes. At the outer edge of the outer blanket, the specific fission rate tends to increase. Such behavior is the result of neutrons that are degraded in energy in the graphite reflector and are scattered back into the breeding blanket.

The distribution of specific Pu^{239} and U^{235} fission rates along the vertical axis of symmetry is given in Fig. 24. Again, a tendency for the U^{235} fission data to flatten at lower and upper portions of the blanket reflects a softening of the neutron spectrum.

Radial and axial comparisons of specific U^{238} fission and capture rates are given in Figs. 25 and 26, respectively. The specific fission rate decreases rapidly with increasing radius as the neutron spectrum becomes softer. The specific capture rate, on the other hand, decreases more slowly and actually increases toward the outer portion of the uranium reflector.

The same information, in the form of α, is given for U^{238} in Fig. 27. The left-hand portion of the figure consists of a radial scan at centerline elevation from the edge of the core to the outer edge of the radial blanket; the right-hand portion consists of traverses along the vertical axis. Again, the softening of the neutron spectrum with penetration into the blanket is manifested by strong changes in the ratio of capture to fission.

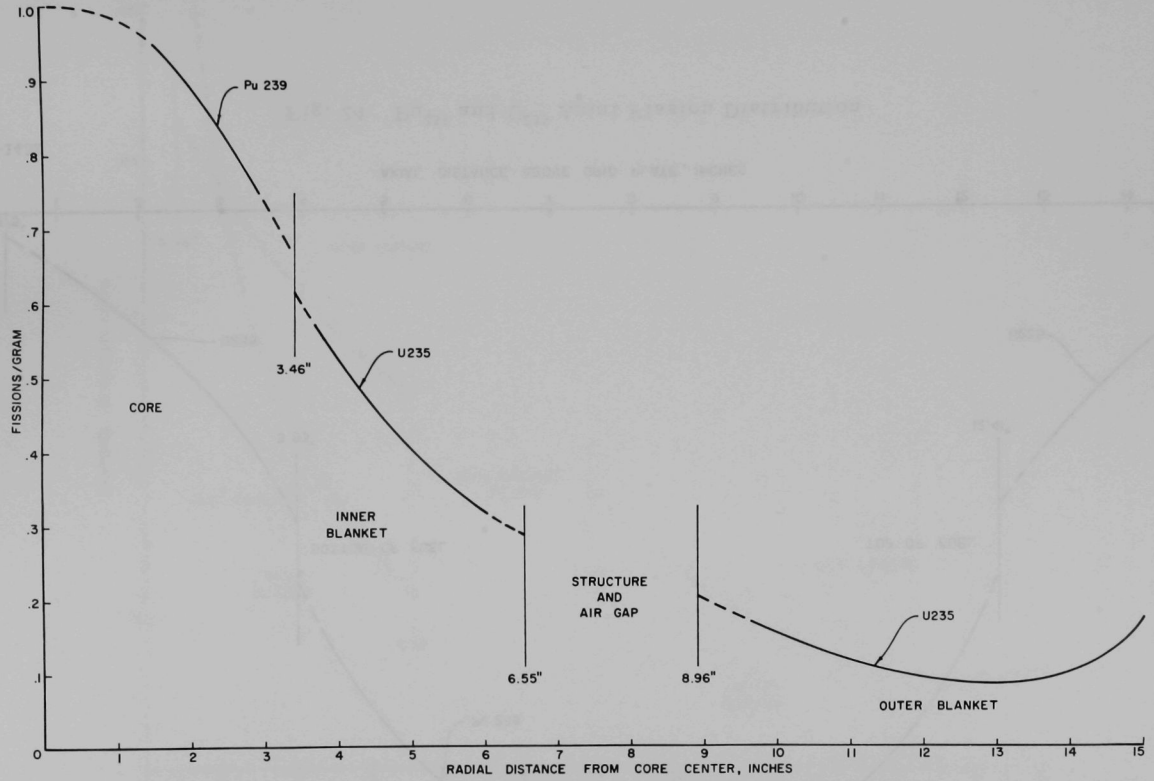

ID-103-1447

Fig. 23. Pu^{239} and U^{235} Radial Fission Distribution

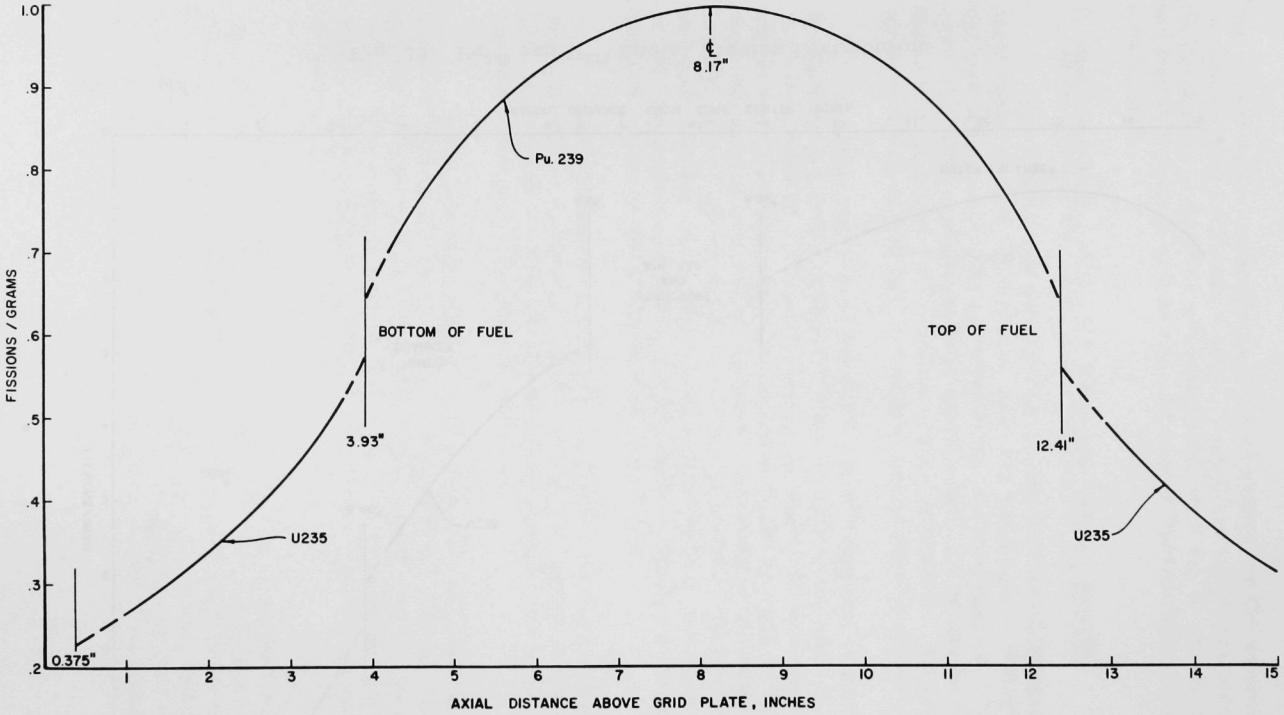

ID-103-1452

Fig. 24. Pu^{239} and U^{235} Axial Fission Distribution

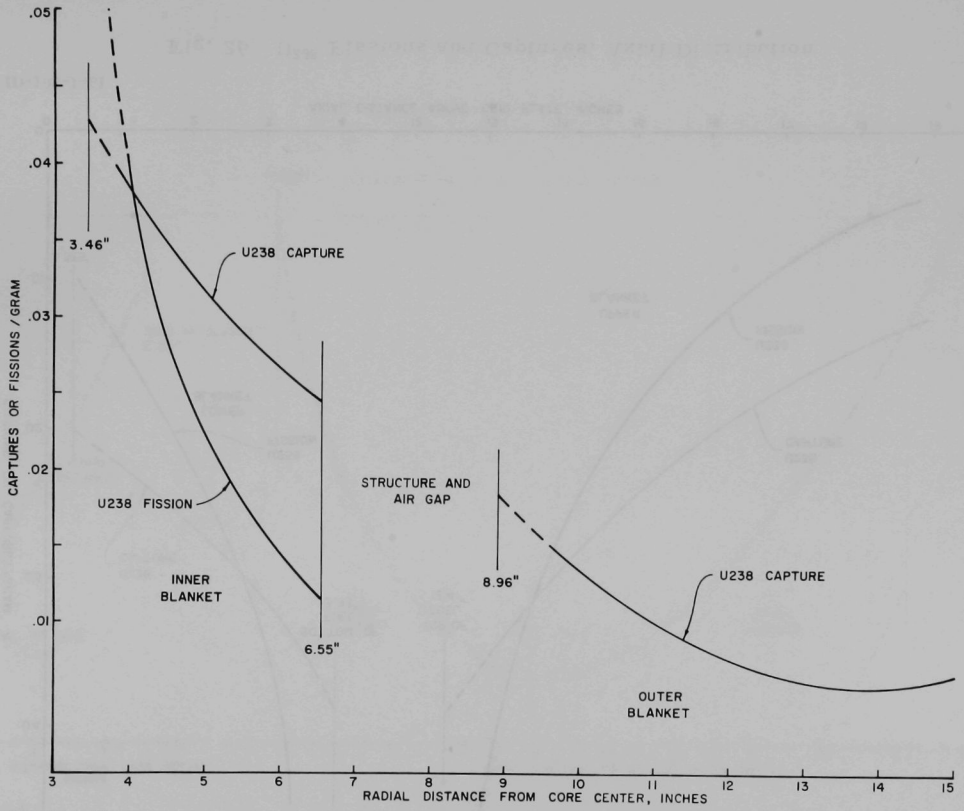

ID-103-1444

Fig. 25. U^{238} Fissions and Captures, Radial Distribution

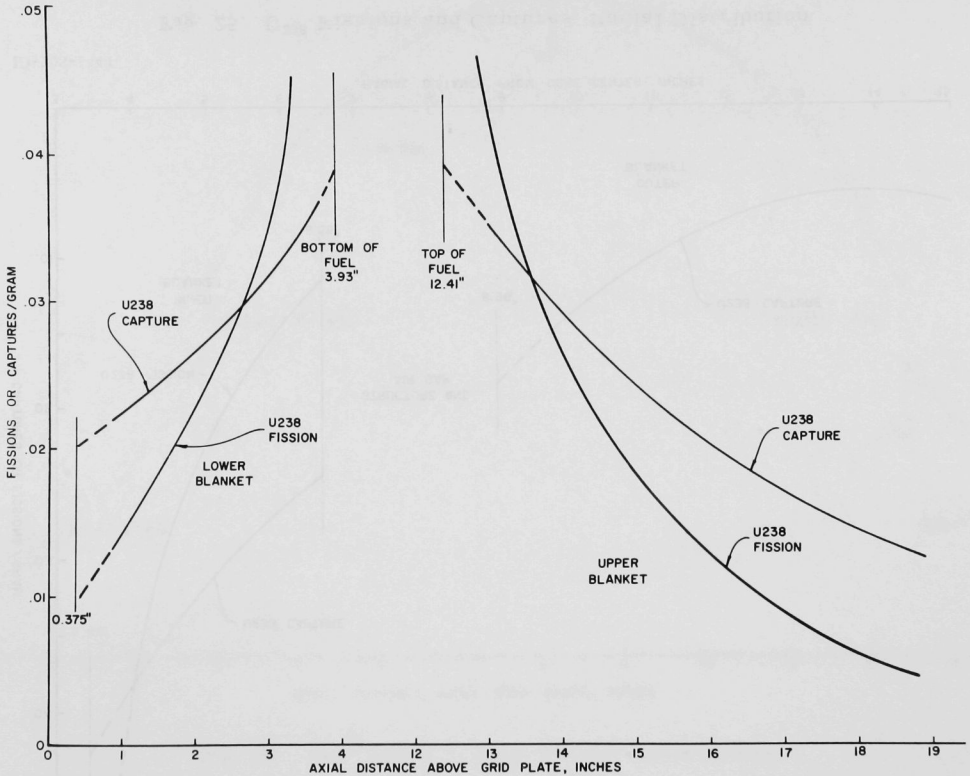

ID-103-1451

Fig. 26. U^{238} Fissions and Captures, Axial Distribution

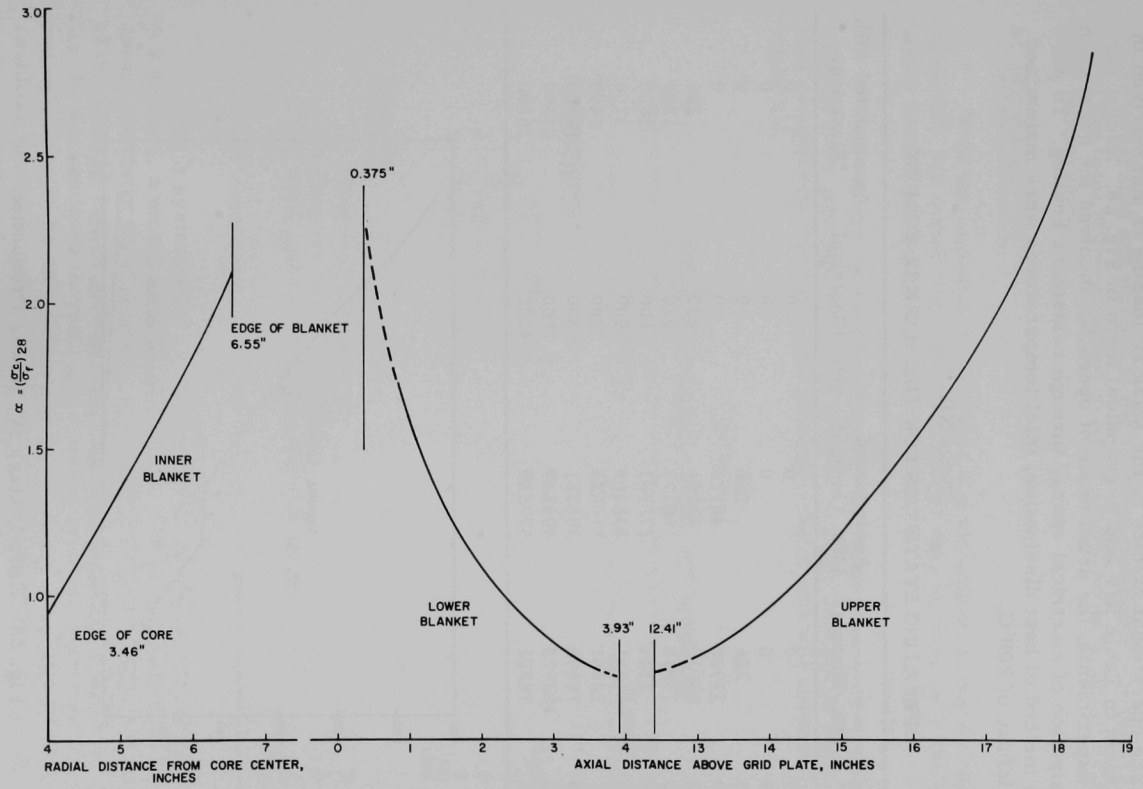

ID-103-1457

Fig. 27. Alpha for U^{238}, Radial and Axial Distributions

V. OPERATIONS

The operational history of the Mark IV loading is summarized in tabular form in Table XIV and in graphical form in Fig. 28. Except for special experiments, the usual mode of operation involved the generation and dissipation of electrical energy through resistance heating. To permit this method of heat dissipation, inlet temperatures were maintained in the vicinity of 200°C.

Table XIV

OPERATING STATISTICS FOR THE MARK IV LOADING

Period Ending	kWh, Thermal	Accumulated kWh, Thermal	kWh, Electrical	Accumulated kWh, Electrical
1/31/63	0	0	0	0
2/28/63	0	0	0	0
3/31/63	206	206	0	0
4/30/63	39920	40126	0	0
5/31/63	53035	93161	230	230
6/30/63	75018	168179	970	1200
7/31/63	8324	176503	600	1800
8/31/63	61861	238364	1900	3700
9/30/63	78261	316625	5700	9400
10/31/63	79696	396321	5400	14800
11/30/63	102928	499249	7100	21900
12/31/63	78201	577350	4200	26100

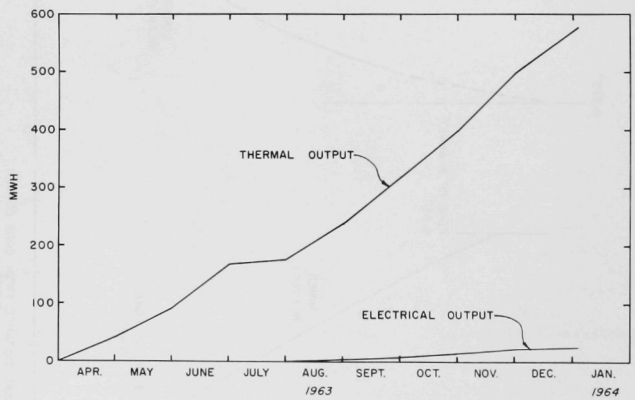

ID-103-1461

Fig. 28. EBR-I, Mark IV, Power Production

The low electrical efficiency indicated from the data of Table XIV and Fig. 28 reflects the consequences of one-shift operation. Before steam can be generated and passed to the turbine-generator, a considerable fraction of the total thermal output must be expended each day in reaching operating temperature.

A. Burnup of Fuel

With the imposition of simplifying assumptions, the values in Table XIV for accumulated thermal output may be used as a basis for evaluating burnup effects in the fuel material.

The energy released in fission is divided among several processes, some of them prompt, and some of them strongly delayed in time. The various components and their approximate magnitudes are summarized in Table XV.

Table XV

ENERGY RELEASE FROM U^{235} FISSION

Process	Energy, MeV
Instantaneous	
1. Fission fragments	168
2. Fission neutrons	5
3. Prompt gammas	5
4. Capture gammas	7
	185
Delayed	
1. Fission-product betas	7
2. Fission-product gammas	6
3. Beta-gammas from capture products	2
	15

For a system such as EBR-I, which operates cyclically (i.e., for 6-8 hr/day), a small fraction of the total energy released will be dissipated during shutdown when power is not being monitored. The remaining fraction of the delayed energy release is automatically considered in the value given for the accumulated thermal output. Assuming an operation of 7 hr/day, for example, it may be shown that the thermal output not considered during the shutdown period is substantially less than 1% of the total and may, accordingly, be neglected.

The amount of fuel destroyed by fission may be found from the accumulated thermal power of 577 MW-hr and the energy release from fission. For this purpose, it will be assumed that the energy released from the fission of Pu^{239}, Pu^{240}, and Pu^{241} is the same as that given in Table XV for U^{235}. It may be shown that the destruction of one gram-atom of either of these species leads to an energy release of 5.3×10^6 kW-hr. Neglecting the small differences in atomic weights, it follows that the fission of 1.08 g of Pu^{239} releases 1 MW-day of thermal energy.

To evaluate the burnup, it is necessary to establish the fraction of the accumulated (monitored) thermal output that originates strictly in the fuel material, since a significant fraction of the monitored output originates in EBR-I from U^{235} and U^{238} fissions in the inner radial-breeding blanket. Information pertinent to such an evaluation is summarized in Table XVI. Listed under column 1 are the various species which, through fission, contribute to the monitored energy release.

Table XVI

DISTRIBUTION OF FISSIONS IN THE CORE AND INNER RADIAL BLANKET, EBR-I, MARK IV

(1)	(2) Fissions[a]	(3) Percentage of Total Fissions
U^{235}	0.026[b] x 10^{18}	2.21
Pu^{239}	0.9146	78.00
Pu^{240}	0.0259	2.21
Pu^{241}	0.0054	0.46
U^{238}	0.2025[b]	17.12

[a]See Table XIII.

[b]Includes fissions in inner blanket only (see Ref. 16).

In all subsequent evaluations, heat-generation effects in the outer reflector will not be considered since the thermal output of this region is not reflected in the values given in Table XIV.

Several definitions of burnup may be given, each of which has a particular significance for a specific reactor. The definition considered most appropriate for EBR-I fuel is essentially that given by Rein,[22] i.e.,

$$\text{APF} = \text{atom percent fission (fuel only)}$$

$$= \frac{\text{number of fissions}}{\text{initial number of heavy atoms}} \times 100. \qquad (8)$$

Neglecting the small mass differences between the various plutonium isotopes, Eq. (8) may be rewritten as

$$\text{APF} = \frac{\text{weight of heavy atoms destroyed by fission}}{\text{initial weight of heavy atoms}} \times 100. \qquad (9)$$

Table XVI indicates that of the total 577 MW-hr of thermal energy, approximately 80.7% originated from the fission of various plutonium isotopes in the fuel material. Using the value of 1.08 g of fuel destroyed per megawatt-day, it follows that the destruction by fission of Pu^{239}, Pu^{240}, and Pu^{241} amounted to 20.2, 0.57, and 0.12 g, respectively, giving a total of 20.9 g. Division of this value by the weight of all heavy isotopes in the operational loading, 2.91×10^4 g, results in an average atom-percent fission burnup of 0.072%.

B. Available Excess Reactivity Anomalies

Before the reactor could be brought to power on any given day, it was necessary, in accordance with standard operational procedure, to establish the total excess reactivity available. Compliance with this procedure assured that any large unanticipated change in reactivity would be revealed at a power slightly above source level. The procedure involved the following steps: (1) establishing critical control positions at low power, (2) determining the excess reactivity available in the system through control-calibration curves, and (3) adjusting the total excess reactivity available to a standard system temperature of 100°C. Day-to-day variations in the system temperature were considered through a correction based on the isothermal temperature coefficient of -3.0 Ih/°C. A considerable backlog of experience indicated that critical positions, adjusted for temperature variations, were usually reproducible on a day-to-day basis within the limits of ±10 Ih. For the Mark IV loading, however, strong anomalies were noted in the daily available excess-reactivity log. An inspection of the data revealed that the anomalies were in some way associated with changes in the coolant inlet temperature.

In particular, operation at about 30°C, following a previous operation at about 230°C, resulted in a reactivity loss of the order of 40 Ih. Conversely, operation of the system at high inlet temperature following a period of low-temperature operation resulted in a comparable gain. To permit an accurate comparison between values measured for the available excess reactivity (i.e., to minimize the effects of temperature corrections), the bulk temperature of the coolant following a hot run was reduced to a value approximately the same as that characterizing the low-temperature runs.

Also considered significant was the fact that operation at full power was not vital to the restoration phenomenon. Merely increasing the bulk

temperature through external heating was sufficient to restore the reactivity loss. The duration of full-power runs had no noticeable influence on the magnitude or characteristics of the anomaly.

Attempts to associate the anomaly with fuel-rod tightness failed. With the tightening rod in all seven fuel assemblies loosened, the associated reactivity loss following high-power, low-inlet-temperature operation amounted to approximately 40 Ih. The loss was, however, regained after running at full power and high inlet temperature. The complete cycle was repeated four additional times. In all cases, the reactivity change was reversible with the amount of change approximately the same as that observed for similar experiments with the rod system tight.

Attempts to associate the reactivity anomalies with subassembly tightness proved successful. All six core clamps, which press inward against the flats of six blanket assemblies, were loosened two turns, or about 26 mils across the diameter of the blanket. The reactivity anomaly (between hot and cold conditions) increased to a reproducible value of approximately 55 Ih. From these results, it seemed likely that the degree of tightness existing between subassemblies had some bearing on the reactivity anomaly.

To explain the anomaly, the following mechanism is postulated. At low inlet temperature and full power, the coolant in the central subassemblies is considerably hotter than the coolant in the outer 12 hexes. Assuming that axial expansion is permitted, the inner assemblies undergo a preferential axial growth. At normal operational power (950 kW and high inlet temperature), the relative growth amounts to approximately 70 mils at seal-plate elevation, and 4 mils at core midplane. If the seal-plate shoes are tight and the core clamps loose, the inner hexes will tend to remain 70 mils higher than the lower support plate after the reactor is shut down. On the other hand, if the seal-plate shoes are loose and the core clamps tight, the vertical displacement of the core, relative to the blanket, will amount to only 4 mils. Under normal operating conditions, both sets of clamps or shoes are nominally tight and the actual vertical displacement of the core after shutdown most likely lies between the two extremes. Such an effect is, of course, strongly negative.

To explain the restoration of reactivity following high-temperature operation (either at power or through external heating), it is necessary to postulate an additional mechanism which acts to loosen the shoes and clamps upon high-temperature operation and which, accordingly, permits the suspended subassemblies to return by gravity to their normal position. A consideration of the following concepts leads to the formulation of such a mechanism.

The operating level of the primary coolant in the reactor tank is maintained constant at the outlet plenum. The temperature of all structural components below this point reflects the effects of changes in the temperature of the inlet coolant. On the other hand, the temperature of upper structural components is not influenced to any significant extent by changes in the inlet coolant temperature.

The actuating rod for the core clamps is located inside a guide tube which dips below the level of the inlet plenum. The pressure of the inlet coolant is sufficient to force inlet coolant up the guide tube, around the actuating rod, and through vent holes at the reactor overflow level. An increase in the temperature of the inlet coolant is manifested by actuating rod expansion, which tends to loosen the core clamps. Calculations based on a 200°C inlet-temperature increase over the length of the actuating rod between outlet and overflow plenums indicate a downward growth of approximately 0.20 in., an amount which loosens the core clamps approximately 70 mils on the diameter.

The actuating rod for the seal-plate shoes is not located in a guide tube. Its temperature above the outlet plenum is essentially that of the surrounding structure. On the other hand, the tie rods that penetrate the upper structure rings are surrounded by spacer tubes, which permit an upward flow and subsequent venting of inlet coolant to the overflow plenum. The expansion of the spacer in the overflow plenum for a 200°C inlet-temperature increase will result in an expansion of the upper structure relative to the actuating rod of 15 mils, an amount which corresponds to a 60-mil diametrical loosening of the seal-plate shoes. Hence, increases in inlet temperature, irrespective of power, are manifested by a loosening of the subassemblies at two points and permit those that have been displaced vertically to fall, by gravity, back to their normal locations. When the temperature of the inlet coolant has been reduced, necessary for an excess available reactivity measurement, the clamps return to their original degrees of tightness. Of the total of 40 Ih associated with the anomaly, approximately 20 Ih can be attributed to the relative movement of the core with respect to the reflector. The remaining 20 Ih is presumably the result of strong end-roughening (end-shape) effects.

The fact that the magnitude of the anomaly decreases when the seal-plate shoes are loosened (with the core clamps held tight) suggests that subassemblies under low inlet-temperature conditions normally tend to "hang up" in the vicinity of the seal plate. Loosening of the seal-plate clamps eliminates such action and leads to a smaller vertical displacement of the core.

A scrutiny of earlier Mark III data leads to the conclusion that similar reactivity anomalies were present during the operation of that loading. But since β_{eff} for Mark III was much larger (0.00685 in contrast with 0.00304),

the anomaly was so small (about 20 Ih) that it was confused at that time with normal day-to-day fluctuations. The fact that such an effect apparently existed in this loading, which structurally is the same, tends to confirm the validity of the mechanisms postulated above.

C. Temperature Measurements

As discussed in Sec. II-C-4, provisions were made for measuring fuel and coolant temperatures at various points throughout the core. Fuel temperatures were measured with stainless-steel-sheathed iron-constantan thermocouples inserted in the fuel. The sheathed leads were accommodated by axial holes bored longitudinally through the rod handles. Coolant temperatures were also measured with the same type of thermocouple inserted in coolant channels at the top of the upper blanket through special tubular handles.

Fuel, blanket, and coolant outlet temperatures for a variety of operating conditions are summarized as a function of radius in Figs. 29 through 31. All fuel temperatures given have been corrected for the effects of the longitudinal hole drilled through the fuel material. While fuel and blanket temperatures are specified for midplane elevation, coolant temperatures apply for an elevation corresponding to the top of the upper blanket.

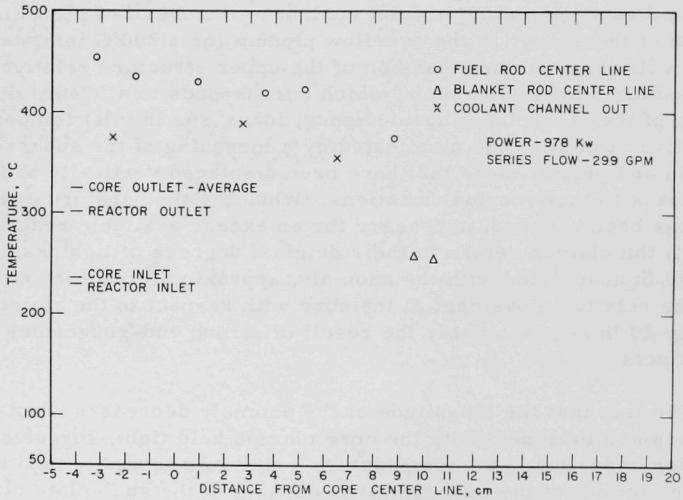

ID-103-1459

Fig. 29. Radial Temperature Distribution at Fuel Vertical Center Line; Power, 978 kW; Flow, 299 gpm

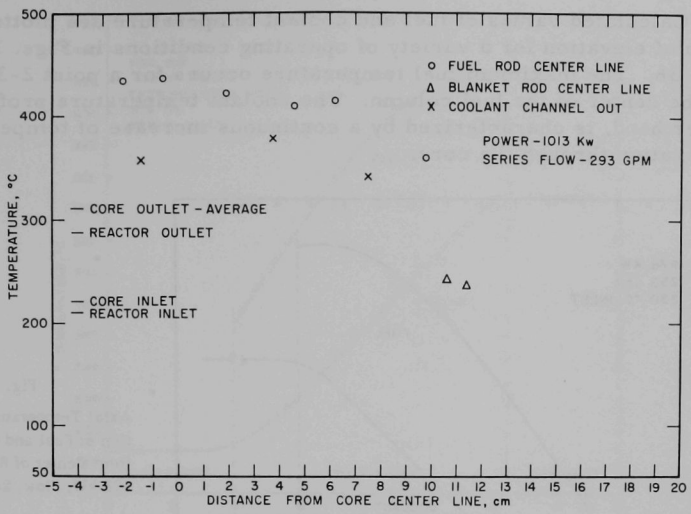

ID-103-1464

Fig. 30. Radial Temperature Distribution at Fuel Vertical Center Line; Power, 1013 kW; Flow, 293 gpm

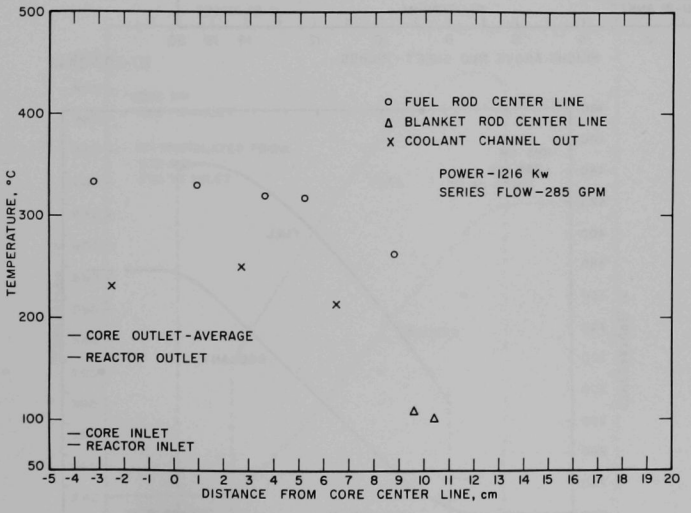

ID-103-1456

Fig. 31. Radial Temperature Distribution at Fuel Vertical Center Line; Power, 1216 kW; Flow, 285 gpm

Calculated values of fuel and coolant temperature are plotted as a function of elevation for a variety of operating conditions in Figs. 32 through 36. The maximum fuel temperature occurs for a point 2-3 in. above the center of the fuel column. The coolant temperature profile, on the other hand, is characterized by a continuous increase of temperature with elevation through the core.

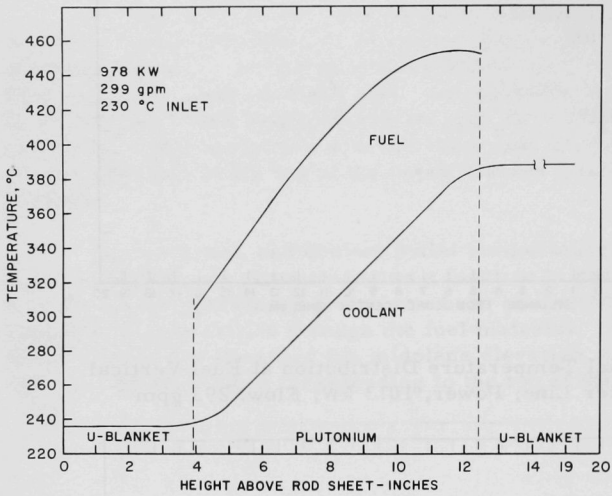

Fig. 32
Axial Temperature Distribution of Fuel and Coolant 1 in. from Center of Reactor; Power, 978 kW; Flow, 299 gpm

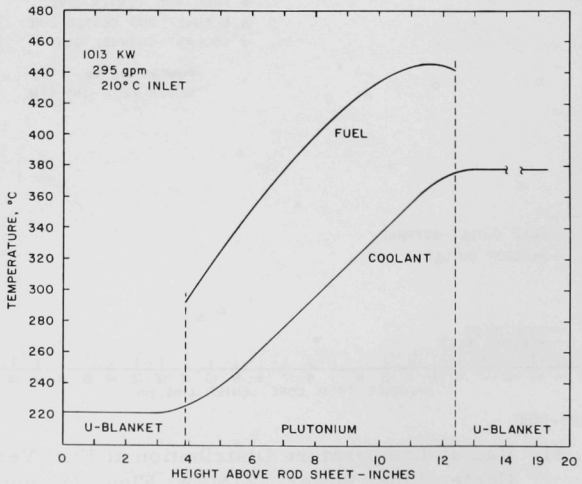

Fig. 33. Axial Temperature Distribution of Fuel and Coolant 1 in. from Center of Reactor; Power, 1013 kW; Flow, 295 gpm

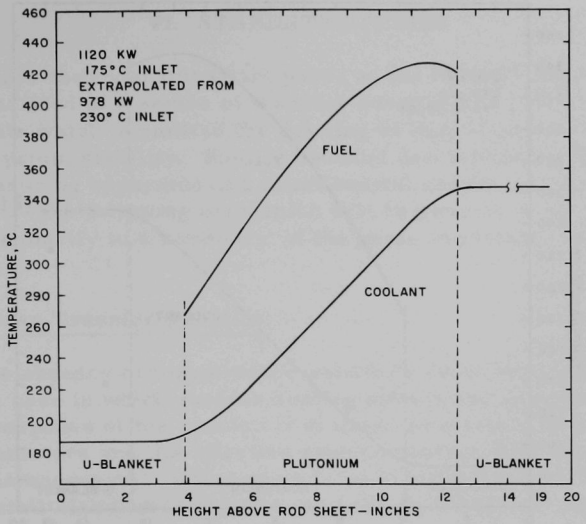

ID-103-1462

Fig. 34. Axial Temperature Distribution of Fuel and Coolant 1 in. from Center of Reactor; Power, 1120 kW; Inlet Temperature, 175°C

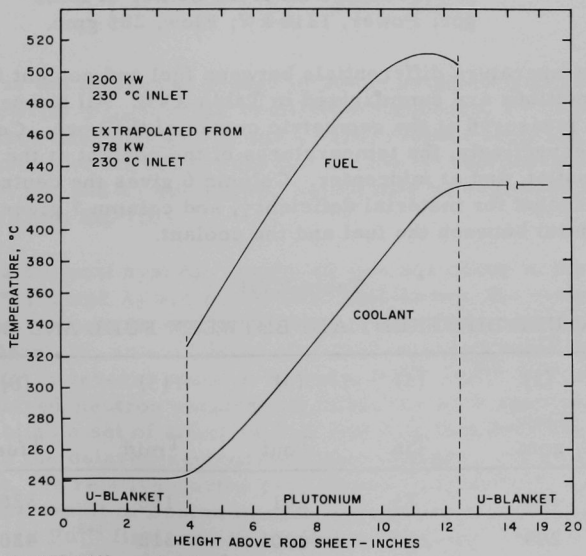

ID-103-1448

Fig. 35. Axial Temperature Distribution of Fuel and Coolant 1 in. from Center of Reactor; Power, 1200 kW; Inlet Temperature, 230°C

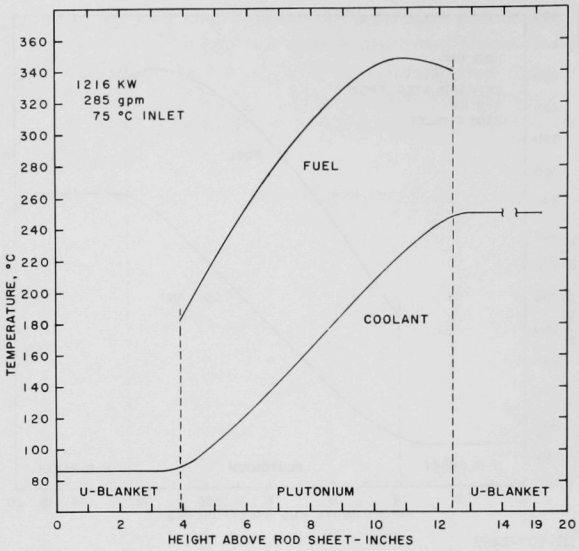

ID-103-1463

Fig. 36. Axial Temperature Distribution of Fuel and Coolant 1 in. from Center of Reactor; Power, 1216 kW; Flow, 285 gpm

The temperature differentials between fuel and coolant for various operating conditions are summarized in Table XVII. All temperatures indicated were measured at the geometric center of the core. Columns 3, 4, and 5 give, respectively, the temperatures of the coolant at the inlet to the core, at the outlet, and at midcenter. Column 6 gives the central fuel temperature corrected for material deficiency, and column 7 gives the temperature differential between the fuel and the coolant.

Table XVII

TEMPERATURE DIFFERENTIALS BETWEEN FUEL AND COOLANT

(1) Power, kW	(2) Flow, gpm	(3) T_{in}	(4) T_{out}	(5) T_{mid}	(6) T_{fuel}	(7) ΔT
1216	285	75	261	168	320	152
978	299	230	400	312	420	133
1013	293	210	388	299	410	132

VI. STABILITY STUDIES

Perhaps the most important phase of the Mark IV experimental program consisted of a series of transfer-function and power-coefficient measurements which permitted the drawing of important conclusions relevant to the system stability. Since a detailed description of the transfer-function measuring apparatus and experimental results has been reported previously,[15] the following discussion will be general in nature and will be limited primarily to a summary of the more important results and conclusions.

A. Zero-power Transfer Function

In the absence of temperature-sensitive reactivity-feedback effects (i.e., for the case in which nuclear heating effects are negligibly small), the kinetic response of the reactor is dictated completely by the delayed-neutron parameters and the effective prompt-neutron lifetime. The development of the necessary mathematics is well-understood and has been treated in detail elsewhere.[25] The expression for the zero-power transfer function is

$$G_0(i\omega) = \frac{\Delta n}{n\rho_{in}} = \frac{1}{i\omega\ell^* \left[1 + \sum_{i=1}^{i=6} \frac{\beta_i}{\ell^*(\lambda_i + i\omega)} \right]} , \qquad (10)$$

where $\Delta n/n$ is the fractional change in power originating from a sinusoidally-varying reactivity ρ_{in}, ω is the oscillation frequency, ℓ^* is the effective prompt-neutron lifetime, and β_i and λ_i are, respectively, the specific relative abundance and the decay constant for the i^{th} delayed-neutron-emitting group. If ℓ^*, β_i, and λ_i are known, $G_0(i\omega)$ may be evaluated as a function of frequency from Eq. (10).

For a thermal system, nearly all fissions occur in the primary fuel, and since ℓ^*, β_i, and λ_i are reasonably well-known, the evaluation of $G_0(i\omega)$, while tedious, is straightforward. For a fast reactor, particularly for EBR-I, Mark IV, an evaluation of $G_0(i\omega)$ is complicated by the fact that fissions occur in several species, namely, Pu^{239}, Pu^{240}, U^{235}, and U^{238}. Since the delayed-neutron parameters differ for each species, it is necessary to establish a set of effective β_i's and λ_i's that describe the average properties of the delayed-neutron-emitting isotopes. As an additional complication, the relative worths of neutrons (both prompt and delayed) emitted as the result of fission in each species must also be considered. Since Pu^{239} and Pu^{240} fissions are limited to the core, while U^{235} and U^{238} fissions are limited to the blanket regions, an evaluation of the relative worths of prompt and delayed neutrons involves a spatial weighting.

Such an evaluation has been carried out by Loewenstein,[26] who has determined the relative number of fissions for each species and the relative worths of prompt and delayed neutrons for a three-region system consisting of a core and two surrounding blankets of different densities. The calculations were carried out for idealized spherical geometry, with consideration given to the replacement of the usual uranium reflector by one of lead. Loewenstein has also evaluated the effective spatially-weighted delay fractions for each species and for each of the six delayed-neutron-emitting groups. Summation over all groups for each of the four species results in an overall effective delayed-neutron fraction of 0.00304.

Effective values of λ_i were established by weighting each value for each species and for each delay group by the fraction of fissions occurring for particular species. The resulting effective parameters for delayed-neutron emission are summarized in Table XVIII.

Table XVIII

EFFECTIVE DELAYED-NEUTRON PARAMETERS FOR EBR-I, MARK IV*

Neutron Group	λ_i, sec^{-1}	β_i
1	0.01294	0.0000904
2	0.03125	0.0007098
3	0.1345	0.0006024
4	0.3348	0.0010613
5	1.286	0.0004357
6	3.361	0.0001452
	Total	0.00304

*After Loewenstein.[26]

The zero-power transfer function was evaluated as a function of frequency from Eq. (10) with the use of an IBM-1620. Input data consisted of values given for β_i and λ_i in Table XVIII and a value of 4×10^{-8} sec for the effective prompt-neutron lifetime. The results for both phase and amplitude are given by the solid curves of Fig. 37. Figure 37 indicates that the agreement between experimentally-determined and theoretically-derived values of the amplitude is satisfactory.

For frequencies greater than 2 cps, a significant difference exists between experimentally-measured and calculated values for the phase of the transfer function. It is also apparent from Fig. 37 that as the frequency increases, the magnitude of the discrepancy becomes larger. The results of previous experiments,[27] in which a similar discrepancy was studied as a function of detector distance, demonstrated that as the detector

is moved away from the core, the discrepancy at a given frequency increases. Covering the detector with 0.030 in. of cadmium foil decreased the discrepancy. Accordingly, the phase discrepancies at high frequencies have been attributed to the time required for neutrons originating in the core to reach the detector. Such a discrepancy, for a given high frequency, is insensitive to power and, once established, may be used as a correction for other data sets. Furthermore, the region of discrepancy, i.e., >2.0 cps, is of little practical interest since feedback effects at these frequencies are essentially nonexistent.

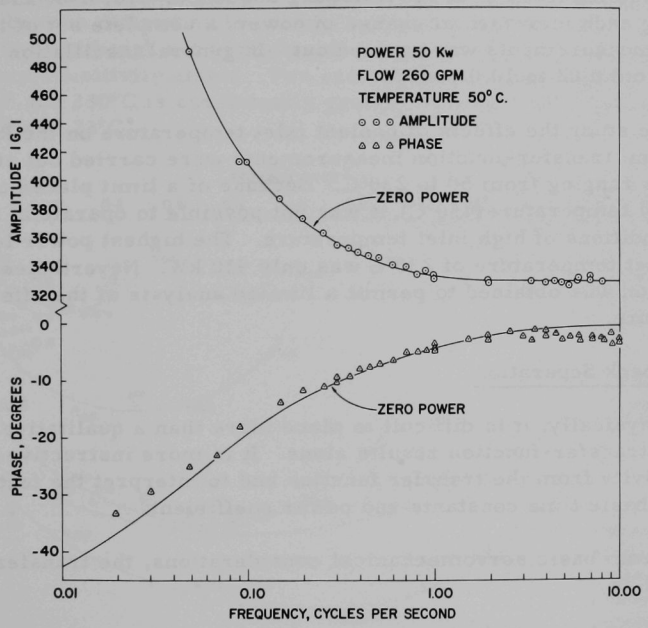

ID-103-1412

Fig. 37. Zero-power Transfer Function

At low frequencies, measured values of the phase are consistently less negative than calculated values. In fact, a definite trend may be noted in the low-frequency phase region with the sense of the discrepancy such that its magnitude increases at the lower frequencies. The origin of this discrepancy has not been established. One obvious explanation, for example, concerns the failure to evaluate properly the effective values of β_i and λ_i used in calculations of the zero-power transfer function.

In separating the feedback from transfer-function measurements, it becomes necessary to choose between the two sets of reference phase

data (i.e., between experimental and calculated values). Since discrepancies of this nature were not experienced in earlier studies conducted with the same equipment, and since the calculated values were based on a series of approximations, it was believed that feedback separations should be based on experimentally-determined values of phase and amplitude.

B. Transfer-function Measurements at Power

The approach to full power (nominally 1200 kW) from cold clean critical was carried out in the following sequence: 510, 878, and 1193 kW. Following each incremental change in power, a complete set of transfer-function measurements was carried out. In general, oscillation frequencies ranged from 0.02 to 10.0 cps.

To study the effects of coolant inlet temperature on the kinetics of the system, transfer-function measurements were carried out at inlet temperatures ranging from 50 to 230°C. Because of a limit placed on the maximum fuel temperature (450°C), it was not possible to operate at full power under conditions of high inlet temperature. The highest power level attained for an inlet temperature of 230°C was only 930 kW. Nevertheless, sufficient information was obtained to permit a limited analysis of the effects of inlet temperature.

C. Feedback Separation

Physically, it is difficult to place more than a qualitative interpretation on transfer-function results alone. It is more instructive to separate the reactivity from the transfer function and to interpret the feedback in terms of basic time constants and power coefficient.

From basic servomechanical considerations, the transfer function is defined as

$$G(i\omega) = \frac{G_0(i\omega)}{1 + G_0(i\omega)\, H(i\omega)}\,, \tag{11}$$

where $G(i\omega)$ is the transfer function under load conditions, $G_0(i\omega)$ is the zero-power transfer function, and $H(i\omega)$ is the reactivity feedback. A rearrangement of Eq. (11) leads to

$$H(i\omega) = [1/G(i\omega)] - [1/G_0(i\omega)], \tag{12}$$

where $1/G(i\omega)$ and $1/G_0(i\omega)$ are the corresponding inverse gains. It is a simple matter to evaluate $H(i\omega)$, since $1/G(i\omega)$ is readily established from the experimental results and $1/G_0(i\omega)$ is available from the calculated zero-power data.

The various feedback results are compared graphically in Fig. 38, in which the real and imaginary components of the feedback are plotted as a function of frequency. Since each data set was obtained under different conditions of power, flow, and temperature, it is difficult to assign any immediate quantitative significance to the results illustrated. Nevertheless, the data, taken collectively, indicate significant trends. The fact that the feedback enters the third (lower left-hand) quadrant at high frequencies indicates that any credible feedback model must be characterized by at least two poles, i.e., two frequency-dependent terms in the denominator. The obvious increase of feedback with power is expected on a purely mathematical basis since feedback is defined as the product of power and the power coefficient of reactivity. Although not particularly obvious from Fig. 38, a strong temperature sensitivity exists. For example, the amplitude of the feedback for 930 kW and 230°C is consistently greater than the amplitude established at 1193 kW and 73°C.

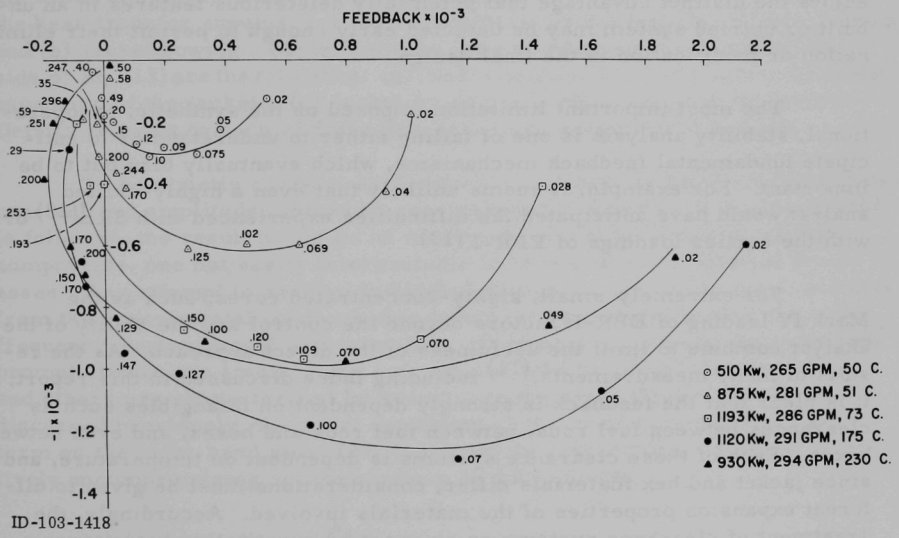

Fig. 38. Comparison of Feedback

D. Feedback Model

The ultimate achievement of feedback analysis would be a detailed, yet understandable, mathematical model which explains all experimentally-observed kinetic phenomena for all conditions of power, coolant flow rate, and temperature. This, of course, is the goal of many analysts, particularly those who are assigned the responsibility of predicting the kinetic characteristics of some postulated system.

The usual approach, in such instances, is one of synthesis. Anticipated reactivity-feedback effects are incorporated into a credible feedback

model which is based, to some extent, on intuition. The substitution of estimates for power coefficients, time constants, damping parameters, etc., into the mathematical model leads eventually to a frequency-dependent feedback which permits an advanced evaluation of the system stability. How successful this approach turns out to be depends strongly on the skill of the analyst and the complexity of the system. In general, it seems reasonable to assume that the original prediction is not perfect. Once experimental information is available, the analyst can return to his synthesis, and by shaping various parameters, force a better agreement between calculated and experimental results. The degree of forcing necessary to effect a satisfactory agreement may then be used as a measure of how well the model was conceived and how accurately the initial parametric values were established. For a satisfactory agreement, the analyst believes, with some justification, that he understands the origins of the various feedbacks, their magnitudes, and their relative phasing. This direct or synthetic approach enjoys the distinct advantage that potentially deleterious features in an unbuilt or untried system may be detected early enough to permit their elimination or modification in the final design.

The most important limitation imposed on the synthetic, preoperational, stability analysis is one of failing either to understand or to anticipate fundamental feedback mechanisms, which eventually turn out to be important. For example, it seems unlikely that even a highly-skilled analyst would have anticipated the difficulties experienced with SRE[28] or with the earlier loadings of EBR-I.[13]

For extremely small, highly-concentrated cores, such as the Mark IV loading of EBR-I, factors beyond the control and the ability of the analyst combine to limit the usefulness of the direct approach. As the results of many measurements,[11] including those discussed in this report, it is clear that the feedback is strongly dependent on intangibles such as clearances between fuel rods, between fuel rods and hexes, and even between hexes. Each of these clearance systems is dependent on temperature, and since jacket and hex materials differ, considerations must be given to different expansion properties of the materials involved. Accordingly, the treatment of clearance systems on an exact or quantitative basis, over a wide range of power and temperature conditions, is not within present capabilities.

As an effective compromise, the analyst may, in such situations, accept the experimental data, and by working backwards, attempt to associate the various feedbacks with temperature-dependent physical processes. In other words, feedback data resulting from a specified set of operating conditions may be broken down into basic time constants and power coefficients, each of which, hopefully, may be identified with a specific feedback mechanism. Finally, if the values of empirically-determined parameters are consistent with those expected from theoretical considerations, the analyst may then feel justified in accepting a mathematical model which describes the feedback function for a limited range of operating conditions.

As a first approximation, the feedback associated with the Mark IV loading may be described by a model which includes two general terms; hence,

$$\text{Total Feedback} = \text{Prompt Feedback} + \text{Delayed Feedback}, \qquad (13)$$

in which the first term defines the feedback associated primarily with power-density changes in the fuel, and the second term describes the feedback associated with expansion effects in the cladding, coolant, and structure. On a relative basis, the first term is prompt and the second term is delayed. The model follows quite closely that proposed by Kinchin,[29] and later extended by Bethe[30] and by Smith et al.[13] to describe the feedback associated with earlier EBR-I loadings.

Contributing to the first term on the right-hand side of Eq. (13) are the following physical effects: (a) expansion of fuel, (b) NaK expulsion from the heat-transfer annulus, (c) radial expansion of the jackets, (d) slug bowing, and (e) jacket bowing. Contributing to the second term on the right-hand side of Eq. (13) are the following: (a) NaK expulsion from the core, (b) radial expansion of the jackets, (c) jacket bowing, and (d) structural expansion. Details relevant to each of these processes are presented in Ref. 15.

To be strictly correct, each effect, along with its characteristic time constant and amplitude, should be considered individually. If this procedure is followed, the result would be an extremely unwieldy series of feedback components, one not easily interpretable in terms of basic physical processes. Any attempt to resolve individual relaxation times and gain constants from the experimental feedback data (which are poorly defined in the high-frequency region) would be impossible. Fortunately, some of the individual prompt effects are small, some pair off and tend to cancel algebraically, and others are characterized by essentially the same time constant. As discussed previously, the exact expansion of the prompt term, [the first term on the right-hand side of Eq. (13)] may be reduced by a series of relatively uncompromising approximations to the following:

$$H(i\omega)\ (\text{prompt}) = \frac{A_0}{1 + i\omega\tau_1}, \qquad (14)$$

where A_0 is the algebraic sum of all prompt reactivity feedback effects that act along a time base approximated by the common time constant, τ_1.

In a similar manner, and for similar reasons, the second term on the right-hand side of Eq. (13) may be reduced to

$$H(i\omega)(\text{delayed}) = \frac{B_0}{(1 + i\omega\tau_1)(1 + i\omega\tau_2)}. \qquad (15)$$

The total feedback sensed by the system is simply the sum of Eqs. (14) and (15); hence,

$$H(i\omega)\ (\text{total}) = \frac{A_0}{1 + i\omega\tau_1} + \frac{B_0}{(1 + i\omega\tau_1)(1 + i\omega\tau_2)} \qquad (16)$$

Essentially, Eq. (16) is the mathematical result of lumping all prompt and all delayed feedback effects into two separate terms. Although both terms have been considerably simplified, it is still clear from Eq. (16) that an empirical evaluation of A_0 and B_0 at low frequencies permits a reasonably accurate comparison of prompt and delayed feedback amplitudes. The phasing of the two terms, relative to the sinusoidal forcing function and to each other, is dictated by the time constants, τ_1 and τ_2. An evaluation of these parameters permits considerable insight into the various feedback processes.

Values established for A_0, B_0, τ_1, and τ_2 from experimental data are summarized in Table XIX.

Table XIX

SUMMARY OF BEST-FIT PARAMETRIC DATA

Power, kW	Flow Rate, gpm	Inlet Temp, °C	A_0, $\Delta k/k$	B_0, $\Delta k/k$	τ_1, sec	τ_2, sec
510	265	50	0.00×10^{-3}	0.515×10^{-3}	0.40	1.78
878	281	51	0.05	1.00	0.50	1.37
1193	286	73	0.10	1.55	0.50	1.41
1120	291	173	0.00	2.30	0.35	2.15
930	294	230	-0.10	2.10	0.40	2.30

An inspection of the parametric data summarized in Table XIX reveals that values for the effective fuel time constant range from 0.35 to 0.50 sec. Each of these is reasonably consistent with the value of 0.50 sec calculated by Mohr[31] for EBR-I, Mark IV, fuel at full power, full flow, and for a low (70°C) inlet temperature. The tendency for the individual values to be lower at higher temperature reflects the increased specific conductivity of the fuel material.

The values extablished for the time constant of the delayed term, although varying from 1.37 to 2.30 sec, are qualitatively consistently with the concept of a transport lag (modified by the Storrer[32] correction) which, for simplicity, has been considered as a simple time constant in the denominator of Eqs. (15) and (16).

A further inspection of the parametric data in Table XIX results in the rather surprising conclusion that in all cases the power coefficient for

the radial (delayed) term exceeds by a very wide margin the power coefficient for the respective axial (prompt) component. In fact, for one data set, that at 930 kW, 294 gpm, and 230°C, the power coefficient for the axial term changes sign. (The convention is such that positive values of A_0 and B_0 result from negative values of the power coefficient. Conversely, negative values result from positive power coefficients.) For reasons discussed in detail elsewhere,[13] A_0 should normally exceed B_0 in importance. The explanation of why A_0 was found to be small, whereas large values were anticipated, is based on the concept of individual fuel slug bowing. Apparently positive reactivity effects associated with slug bowing were large enough to cancel the normally-expected negative effects arising from axial expansion, NaK expansion, etc. Evidence strongly substantiating slug bowing as a mechanism was supplied by a series of static power-coefficient measurements.

E. Effect of Inlet Temperature on Feedback

The data presented in Fig. 38 indicate that variations in the inlet temperature cause strong changes in the amplitude of the feedback. Unfortunately, it is difficult to assess the true magnitude of the inlet-temperature effect from the data of Fig. 38, since each data set was obtained under different conditions of power and coolant flow. To obtain a more realistic estimate of the inlet-temperature effect, it is instructive to normalize the data from two sets to that of a third. If as a first approximation it is assumed that the feedback varies directly as the power and inversely as the flow rate, the data sets for 1120 and 930 kW were normalized to the data set at 1193 kW. Neither assumption is seriously compromising since the differences in flow rates between sets are small, and the power coefficients of reactivity in the region of interest are, to a first approximation, linear.

The results of the normalization are given in Fig. 39. Of particular interest is the fact that increasing the inlet temperature from 73 to 175°C results in a large increase in the magnitude of the feedback. Yet, an additional increase to 230°C apparently has little effect. A credible interpretation of these effects is one based on a temperature-sensitive system of clearances. With the inlet temperature low (i.e., about 30°C), it is reasonable to assume that clearances between fuel rods, between fuel rods and hexes, and between hexes are at a minimum, since the core clamps and the expandable tightening rods were adjusted under these conditions. Except for mechanical imperfections in the rods, the core may be regarded as a tightly-coupled system of individual rods. In principle, a rib-to-cladding contact exists uniformly throughout the system. If the power is increased without changing the inlet temperature, the jackets will tend to expand radially; but since the temperature of the structure rings and the outer row of 12 blanket subassemblies remains at inlet temperature, the full radial component of jacket expansion will not be realized. Under these conditions the power coefficient will reflect a decrease proportional to the constraining

effect. In practice, small radial clearances most likely exist, even under idealized tightened conditions, and the radial component will certainly not be zero.

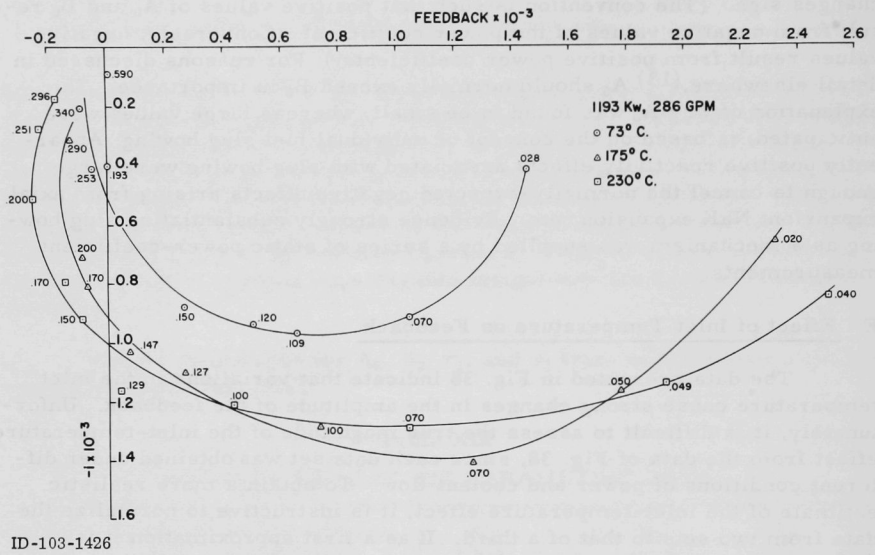

Fig. 39. Inlet Temperature Effect

If the temperature of the inlet coolant is raised to 73°C to conform with the data of Fig. 39, all stainless-steel components including the hexes and structure rings will expand by an amount dictated by the expansion coefficient of stainless steel ($18.4 \times 10^{-6} \Delta L/L/°C$). Jacket material will also expand, but since the expansion coefficient of Zircaloy-2 ($9.6 \times 10^{-6} \Delta L/L/°C$ is much smaller, the effect of an overall increase in temperature (at zero power) will be one which tends to open various clearance systems. Under these conditions, more "room" is available to accept a colligative radial expansion, with the result that the radial component of the power coefficient is strong. If, however, the power is increased indefinitely, clearances will gradually close until the constraining influence of the outer hexes is again felt. At this point in power, the radial component of the power coefficient will decrease.

Moderate additional increases in the temperature of the inlet coolant will result in additional increases in radial clearances. The results, as demonstrated by the data of Fig. 39, are reflected by an increase in the power coefficient. At even higher temperatures, clearances between rods and between rods and hexes will be such that even at full power, constraining effects will not be felt; i.e., enough room will exist to accept the full

unconstrained effects of radial expansion. For these special conditions, the radial component of the power coefficient will reach its maximum. From Fig. 39 it seems likely that the "saturation" inlet temperature lies between 175 and 230°C, since the increase between these values effects a relatively small, perhaps insignificant, increase in the magnitude of the feedback.

The effect of inlet temperature on feedback behavior introduces the interesting possibility that further increases (above saturation) in inlet temperature may lead to a decrease in the radial component of the power coefficient. If, for example, the clearances between fuel rods and between fuel rods and hexes increase to the extent that the core becomes completely uncoupled, the radial effects of jacket expansion may no longer be a colligative property. Under such, by no means incredible, conditions, the power coefficient may actually decrease to a value comparable in magnitude to that associated with the completely coupled and perfectly constrained core.

F. Nyquist Stability Criterion

A measure of the stability of the system may be obtained from the application of the Nyquist stability criterion. Since the transfer function $G(i\omega)$ is defined by

$$G(i\omega) = \frac{G_0(i\omega)}{1 + G_0(i\omega)\, H(i\omega)}, \qquad (17)$$

the amplitude of the transfer function approaches infinity as the product $G_0(i\omega)\, H(i\omega)$ approaches -1.

If it is assumed that feedback varies linearly with power, $G_0(i\omega)\, H(i\omega)$ may be evaluated as a fraction of frequency for increasing levels of power. The result is a family of curves which approaches the (-1, 0) point as power is increased. An illustration of the principle is given in Fig. 40. The feedback is in all cases that established experimentally for 1120 kW, 291 gpm, and 175°C. The intersection of the various $G_0(i\omega)\, H(i\omega)$ curves with the constant-frequency lines gives the value of $G_0(i\omega)\, H(i\omega)$ for a particular frequency at some specific multiple of 1120 kW (full power). Figure 40 indicates that the system is stable for all credible levels of power. A continuous increase in power beyond $10P_0$ (ten times nominal full power) could conceivably bring $G_0(i\omega)\, H(i\omega)$ into coincidence with the (-1, 0) point. The power level necessary to effect coincidence, however, would be an absurdity, considering limitations imposed by melting points and capabilities for heat removal. In a practical sense, the system could never be made unstable by a continuous power increase.

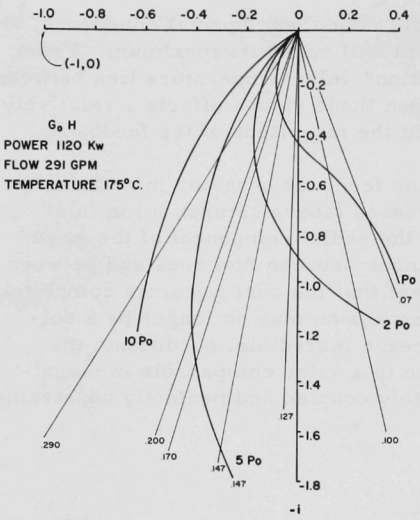

ID-103-1427

Fig. 40. Nyquist Stability Criterion

G. Extrapolation of the Transfer Function

Essentially the same information, but in transfer-function form, is given in Fig. 41. The upper family of curves defines the amplitude for various multiples of full power. It is interesting to note that as the power increases, the resonance peak increases in magnitude, sharpens in definition, and moves in the direction of higher frequencies. Even at $10P_0$, the increased amplitude poses no operational problem.

The lower family of curves gives the phase of the transfer function as a function of frequencies for various multiples of power. The most significant features are a strong tendency for phase values to become more positive and a decided shift in the phase peak towards higher frequency. Although not illustrated, each of the other data sets, when extrapolated, gives essentially the same information.

Fig. 41

Extrapolated Transfer Functions

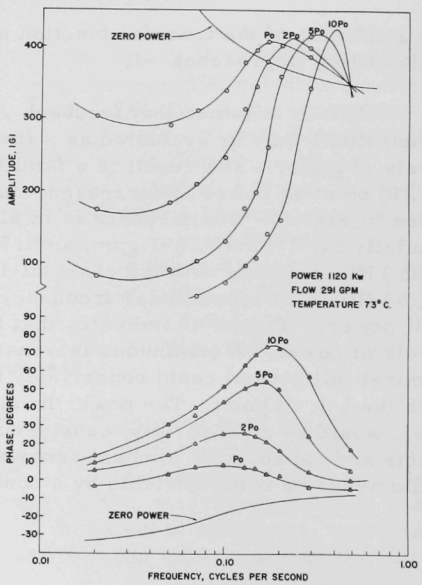

ID-103-1428

H. The Effect of β_{eff} on Stability

The effects of a low value of β_{eff} (0.00304, in contrast with 0.00685 for a similar U^{235} loading) on the kinetic behavior is illustrated in Figs. 42 and 43. The first of these illustrates the case for a feedback that interferes

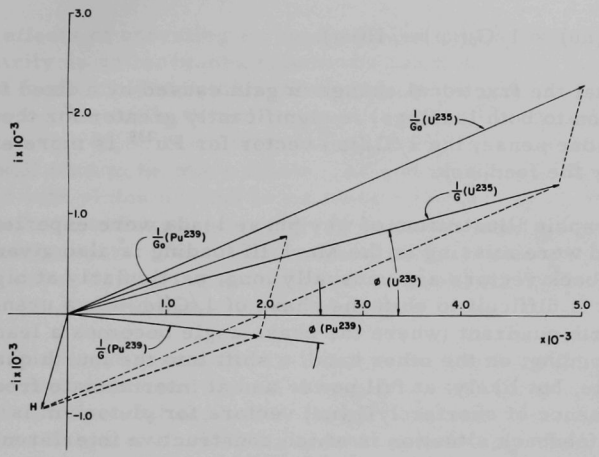

ID-103-1429

Fig. 42. The Effect of Third Quadrant Feedback on Stability

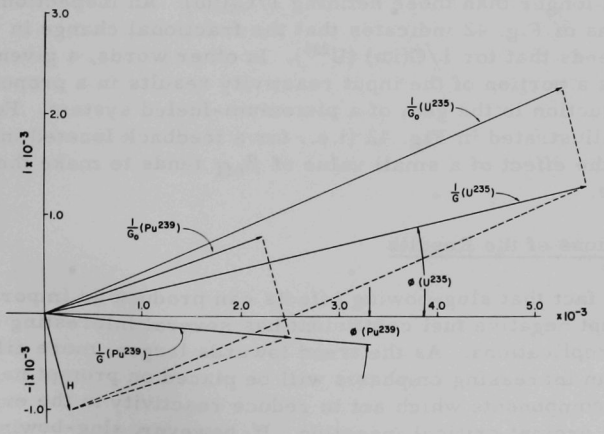

ID-103-1430

Fig. 43. The Effect of Fourth Quadrant Feedback on Stability

constructively with the reactivity input; i.e., the phase is such that feedback reinforces the input. Shown in vector form are the feedback $H(i\omega)$ and the inverse zero-power gains associated with plutonium and uranium loadings. All three vectors have been evaluated at the same frequency. Since the inverse gain is simply

$$1/G(i\omega) = 1/G_0(i\omega) - H(i\omega), \tag{18}$$

it follows that the fractional change in gain caused by a fixed feedback (i.e., common to both loadings) is significantly greater for the plutonium loading. In one sense, the $1/G_0(i\omega)$ vector for Pu^{239} is more effectively cancelled by the feedback.

A graphic illustration of why phase leads were experienced in Mark IV and were missing in the Mark III loading is also given in Fig. 42. Unless feedback vectors are unusually long, particularly at higher frequencies, it is difficult to shift the phase of $1/G(i\omega)$ for a uranium loading into the fourth quadrant (where the phase angle becomes a lead). For a plutonium loading, on the other hand, a shift into the fourth quadrant is not only possible, but likely, at full power and at intermediate frequencies. The consequence of shorter $1/G_0(i\omega)$ vectors for plutonium is essentially this: for a feedback situation in which constructive interference is possible, a small value of β_{eff} tends to make the system less stable.

The converse situation, in which the feedback reactivity cancels a portion of the input, is illustrated in Fig. 43. In both cases, the $1/G(i\omega)$ vectors are longer than those defining $1/G_0(i\omega)$. An inspection of the vector diagrams of Fig. 42 indicates that the fractional change in $1/G(i\omega)$ (Pu^{239}) exceeds that for $1/G(i\omega)$ (U^{235}). In other words, a given feedback that cancels a portion of the input reactivity results in a proportionately greater reduction in the gain of a plutonium-fueled system. For the conditions illustrated in Fig. 42 (i.e., for a feedback located in the fourth quadrant), the effect of a small value of β_{eff} tends to make the system more stable.

I. Implications of the Results

The fact that slug-bowing effects can produce an important reduction in the prompt negative fuel coefficient has several interesting and perhaps important implications. As the trend towards larger, more dilute, cores continues, an increasing emphasis will be placed on prompt negative power coefficient components which act to reduce reactivity in the event of an inadvertent prompt critical insertion. If, however, slug-bowing and jacket-bowing effects are sufficiently large, they may greatly reduce or even override prompt negative effects associated with Doppler broadening and axial fuel expansion. For these special, but not improbable, conditions, the system would be left with little or no inherent shutdown capability.

Since the fuel in EBR-II also consists of sodium-bonded slugs,[33] it is possible that bowing may affect the kinetic response of the system to a measurable degree. Although it is highly unlikely that such effects will introduce operational problems, it is reassuring, in some respects, to be aware of this interesting possibility.

The effects of operating a system fueled with plutonium are manifested primarily as an increased sensitivity towards reactivity perturbations. For a feedback that reinforces the input, the neutron kinetics are such that the system tends to be less stable (relative to the case for U^{235} fuel). On the other hand, for a feedback that cancels a portion of the input, the system will tend to be more stable. As a consequence, for a reactor that is fueled with plutonium and is inherently stable, effects that tend to counteract transient changes in reactivity act more strongly than in the U^{235}-fueled counterpart. Therefore, normal perturbations in reactor power which occur during the operation of a reactor should be smaller in magnitude for the plutonium-fueled reactor.

As a final implication, the fact that power coefficients in small, high-power-density systems depend strongly on clearances, bowing effects, and differential structural expansion should be of interest to the designers of space-oriented systems. Failure to anticipate strong nonlinearities in the power coefficient and reversals of sign could result in poorly-designed and perhaps inadequate systems of control.

VII. FISSION-PRODUCT MONITOR

In the event of a fuel-element failure (cladding rupture) in EBR-I, minute quantities of fission products will be released directly to the NaK coolant. For a minor failure, there is no compelling reason why normal operations should be interrupted. Since the primary NaK coolant is normally highly radioactive (mainly from Na^{24}), the contribution to the specific activity of the coolant from a credible fission-product release will be essentially immeasurable. All primary components are heavily shielded and are inaccessible during and following (for approximately one week) a normal operating period. In principle, the reactor could be operated indefinitely with essentially no aggravation of personnel-monitoring problems.

For a serious failure or for a series of small failures, however, continued operation may lead to a fission-product accumulation sufficiently large to affect the accessibility of primary components for occasional maintenance. From the operational point of view, some system capable of annunciating and analyzing the seriousness of a cladding failure is a necessity. On the basis of information gleaned from such a system, the operator may elect either to continue operation or to shut down, locate, and replace the damaged rod. Accordingly, a modest effort was devoted to the development and testing of a device which seemed capable of promise not only for EBR-I but for other Na- or NaK-cooled future fast systems.[34]

A. Monitoring Principle

The problem of annunciating the presence of fission products in a Na or NaK coolant through observation of fission-product beta-gamma activities is essentially one of detecting a small signal in the presence of an overriding noise associated with the beta-gamma activity of Na^{24}. Advantage may be taken of the fact that certain fission products emit delayed neutrons. Suitable neutron detection equipment installed at a downstream location should, in principle, be capable of annunciating the presence of fission products. A monitoring system based on delayed-neutron detection is currently being installed at EBR-II; future testing under actual operating conditions will permit a realistic appraisal of its applicability.

The necessity of blanketing the primary coolant in a fast reactor with an inert gas such as argon, however, suggests another interesting possibility, since it is known that rare-gas fission products (krypton and xenon) diffuse rapidly into the cover-gas system. In principle, some suitable beta-gamma detector which monitors the activity of the cover gas should be capable of annunciating a cladding failure. In practice, it is necessary to effect an almost complete discrimination against A^{41}, which is present in the cover gas at activity levels many orders of magnitude higher than those associated with credible concentrations of rare-gas fission products.

A simple and extremely efficient method of discrimination against A^{41} was developed and tested, a method which utilizes the selective electrostatic fixation of rare-gas daughter nuclides. The principle of the fixation process is premised on the fact that at the instant of beta decay, each of the daughter species becomes a positively-charged ion. Accordingly, the cover gas is passed through an electrostatic precipitation unit, which consists primarily of a cylinder maintained at a potential of 2500 V positive. A closed-loop wire, driven axially through the cylinder, is maintained at ground. Upon beta decay, the ionized daughter species migrate to the wire and become electronically neutralized. The wire carrying the neutralized daughters passes through a mercury trap-type gas seal which had a few milliliters of water floating on its surface. The strongly electropositive rubidium and cesium daughters react instantly with the water and become permanently fixed in the water layer in the hydroxide form. The isotope K^{41}, the daughter of A^{41}, also reacts with the water, but since K^{41} is radioactively inert, the activity associated with the water fraction is almost exclusively that arising from the decay of various rubidium and cesium fission products. It follows that the output from a detector that monitors the activity level of the water fraction may be used as a criterion of the fission-product concentration in the cover gas. Details relevant to the precipitation apparatus and the detection equipment (a NaI scintillator unit) have been given previously.(34)

B. Test Results

The testing of the equipment in EBR-I was complicated by the fact that under normal operating conditions, substantial quantities of rare-gas fission products are released continuously to the cover gas from the following sources: (1) vented blanket thermocouple rods, and (2) a small, unknown, uranium contamination in the NaK coolant. Obviously, the natural existence of fission products in the system reduces the sensitivity and the effectiveness of the system. On the other hand, the continuous release of fission products from these sources provided an opportunity to evaluate the performance of the equipment under the realistic conditions of actual operation.

For the monitoring system described above, the possibility exists that A^{41} may be carried over into the downstream (monitored) trap, through diffusion, through sorption into the stainless-steel wire, or through some unsuspected mechanism. To test for this possibility and to assess the degree of discrimination against A^{41}, 0.1 ml of water was taken from the trap after 2 hr of full-power operation and analyzed with a NaI 256-channel pulse-height analyzer. The results are given in Fig. 44. Each of the gamma peaks may be identified with radiations associated with specific isotopes of rubidium and cesium. From the spectrum, it is clear that the 1.29 MeV gamma of A^{41} is almost completely missing and that the degree of discrimination against A^{41} is satisfactorily high.

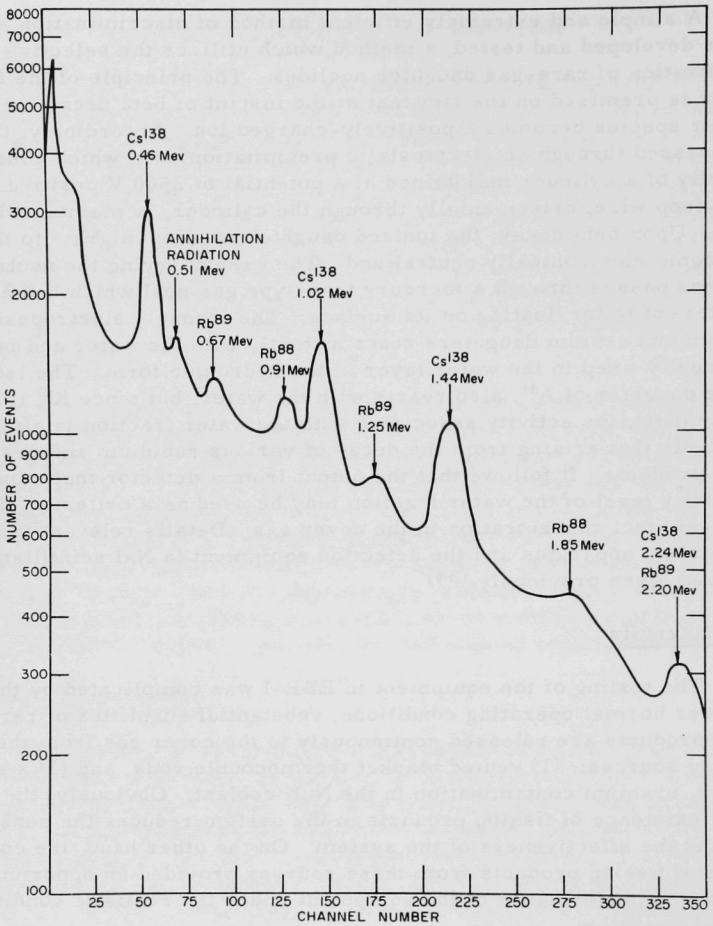

ID-103-1401

Fig. 44. Pulse-height Spectrum of Water Fraction

As the spectrum of Fig. 44 indicates, essentially all the activity associated with the water fraction is the result of the decay of three fission-product species, i.e., Rb^{88}, Rb^{89}, and Cs^{138}. The half-lives of the species are short, being, respectively, 18, 15 and 32 min. In addition, the respective half-lives of their precursors are also short, i.e., 2.8 hr, 3.2 min, and 32 min. It follows that the decay of precursors and daughters will be essentially complete for shutdown periods longer than a few hours. During a startup following a prolonged shutdown (overnight, for example),

it is clear that the activity level of the water fraction will increase rapidly from zero and will eventually reach equilibrium at a time dictated by the half-lives of the rare gases, their precursors, and their immediate daughters.

To evaluate the feasibility of differentiating the effects of fission-product release during a cladding failure from those associated with normal release, it was necessary to separate the saturated normal response into the following components: (1) environmental background, (2) reactor background, (3) A^{41} background, and (4) the normal rubidium-cesium signal. Since details of these measurements have been given previously,(34) it is sufficient merely to cite the actual results, listed in Table XX. From Table XX, it may be seen that the ratio of normal rubidium-cesium activity to the sum of all other background components is approximately 0.58. Similar measurements carried out with a previous loading (Mark III) resulted in a ratio value of 8.0. The striking difference reflects the removal of 12 vented fuel thermocouple rods which released approximately 14-fold greater quantities of fission products to the coolant.

Table XX

INTENSITY OF BACKGROUND COMPONENTS, EBR-I, MARK IV

Component	Source	Intensity, cps
1	Environmental	4
2	Reactor	36
3	A^{41}	0
4	Rb-Cs	23
Total	All Sources	63

To obtain some realistic measure of the time response and the strength of the signal resulting from the failure of a typical fuel rod, a simulation experiment was carried out. Twenty unclad enriched uranium foils, each 1 x 1 cm, were packed into a NaK-ventilated basket which, in turn, was installed near the edge of the core in a NaK-ventilated thimble. The combined area of the 20 foils was chosen to coincide with the exposed area of fuel in a typical Mark IV fuel rod.

The results of measurements conducted at 900 kW (full power, 1200 kW) are illustrated in Fig. 45, which gives the activity associated with the water layer as a function of time after reaching operating power. The lower curve, obtained under normal operating conditions, gives a true measure of the background level. As expected, the activity, extremely low shortly after startup, increases rapidly and eventually reaches saturation approximately 3 hr after startup. Repeat measurements conducted on three successive days demonstrated the reproducibility of the results.

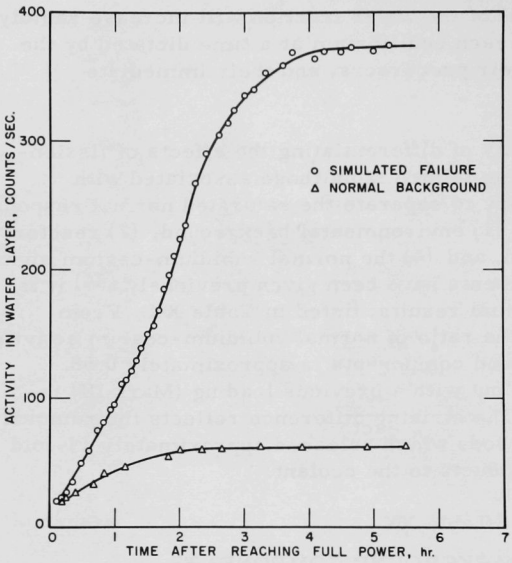

ID-103-1401

Fig. 45. Fuel-rod Failure Simulation, EBR-I, Mark IV

The upper curve of Fig. 45 gives the results of measurements carried out with the unclad enriched uranium foils in position and and with all other conditions unchanged. Hence, for any given time, the intensity difference between the two curves gives a measure of the fission-product release from the unclad foils. To permit a reasonable evaluation of the effect expected from the failure of a single Mark IV fuel rod, corrections for the difference between Pu^{239} and U^{235} fission cross sections have been applied to the data illustrated.

From the results of Fig. 45, it is clear that the strength of the fission-product signal from the simulated failure is approximately five times that of the normal (combined) background signal. It is reasonable to conclude, from the results of this somewhat idealized experiment, that the release of fission products from the failure of a single Mark IV fuel-rod cladding would be detectable.

ACKNOWLEDGMENTS

The authors gratefully acknowledge the assistance of the following individuals: F. S. Kirn, who participated in the approach-to-critical experiments; R. A. Horne, APDA, Detroit, Michigan, who assisted with the breeding-gain measurements; and R. D. DeForest, who helped with the transfer-function measurements. The cooperation and assistance of the EBR-I operating crew, consisting of Larry Hill, Jerry Cockerill, Floyd Butler, Ken Detroit, and Curtis Tidmore, are also gratefully acknowledged.

REFERENCES

1. Zinn, W. H., et al., Feasibility Report, Fast Neutron Pile for Test of Conversion, ANL-4356 (Oct 1949).
2. Lichtenberger, H. V., et al., Experimental Breeder Project Report for the Period December 1, 1948 through February 1949, ANL-4274.
3. Lichtenberger, H. V., et al., Experimental Breeder Project Report for the Period March 1, 1949 through January 31, 1949, ANL-4420.
4. Lichtenberger, H. V., et al., Experimental Breeder Project Report for the Period February 1, 1950 through March 31, 1951, ANL-4554.
5. Lichtenberger, H. V., et al., Experimental Breeder Project Report for the Period April 1, 1951 through January 31, 1953, ANL-5023.
6. Lichtenberger, H. V., Operating Experience and Experimental Results Obtained from a NaK-Cooled Fast Reactor, Proceedings of the International Conference on the Peaceful Uses of Atomic Energy, United Nations, New York, 6, 345 (1955).
7. Jens, W. H., and Klecker, R. W., EBR Transfer Function Experiment, unpublished.
8. Brittan, R. O., Analysis of the EBR-I Core Meltdown, Proceedings of the Second United Nations International Conference on the Peaceful Uses of Atomic Energy, Geneva, Switzerland, 12, 267 (1958).
9. Kittel, J. H., et al., The EBR-I Meltdown--Physical and Metallurgical Changes in the Core, Nucl. Sci. Eng. 4(2), (Aug 1958).
10. Rice, R. E., et al., EBR-I, Mark III Design, ANL-5836 (March 1958).
11. Smith, R. R., et al., Instability Studies with EBR-I, Mark III, ANL-6266, (Dec 1960).
12. Thalgott, F. W., et al., Stability Studies on EBR-I, Proceedings of the Second United Nations International Conference on the Peaceful Uses of Atomic Energy, Geneva, Switzerland, 12, 242 (1958).
13. Smith, R. R., et al., A Mechanism Explaining the Instability of EBR-I, Mark II, ANL-6354 (Sept 1961).
14. Haroldsen, R. O., et al., Safety Analysis Report, EBR-I, Mark IV, ANL-6411 (Feb 1963).
15. Smith, R. R., et al., Stability Considerations for a Plutonium Loading in EBR-I, ANL-6863 (May 1964).
16. Smith, R. R., et al., The Breeding Ratio of a Plutonium Loading in EBR-I, ANL-6789 (Feb 1964).
17. Baker, A. R., Argonne National Laboratory, unpublished work.

18. Kato, W. Y., et al., Measurements of the Conversion Ratio for a Fast Breeder Reactor, First Nuclear Engineering and Science Congress, Cleveland, Ohio, Vol. II, Reactor Operational Problems, Pergamon Press, New York (1957).

19. Kafalas, P., et al., Determination of the Ratio of Capture to Fission Cross Sections in EBR-I, Nucl. Sci. Eng. 2(5), 657 (1957).

20. Yiftah, S., et al., Fast Reactor Cross Sections, Pergamon Press, New York (1960).

21. Davey, W. G., Argonne National Laboratory, private communication.

22. Rein, J. E., Phillips Petroleum Company, private communication.

23. Armani, R. J., Argonne National Laboratory, private communication.

24. Okrent, D., and Thalgott, F. W., Proceedings of the Conference on Plutonium as a Power Reactor Fuel, HW-75007 (Dec 1962).

25. Schultz, M. A., Control of Nuclear Reactors and Power Plants, McGraw-Hill Book Company, Inc., New York (1955).

26. Loewenstein, W. B., Argonne National Laboratory, private communication.

27. Boland, J. F., A Measurement of the Transfer Function of a Fast Critical Facility, ANL-5782 (Sept 1957).

28. Donohue, H. F., and Keaton, W. W., Fuel Rod-bowing in SRE, NAA-SR-6878 (June 1962).

29. Kinchin, G. H., The Stability of Fast Reactors, RP/M83, AERE, Harwell (June 1956).

30. Bethe, H. A., Reactor Safety and Oscillator Tests, APDA-117 (Oct 1956).

31. Mohr, D., private communication (Jan 1964).

32. Storrer, F., Temperature Response of Power, Inlet Coolant Temperature and Flow Transients in Solid Fuel Reactors, APDA-132 (June 1959).

33. Koch, L. J., et al., Addendum to Hazard Summary Report, EBR-II, ANL-5719 (May 1957).

34. Smith, R. R., and Doe, C. B., Fission Product Monitoring in EBR-I, Mark IV, ANL-6788 (Jan 1964).